

QUANTIFYING THE HEAT STORED IN URBAN ENVIRONMENTS USING REMOTE SENSING TECHNOLOGY

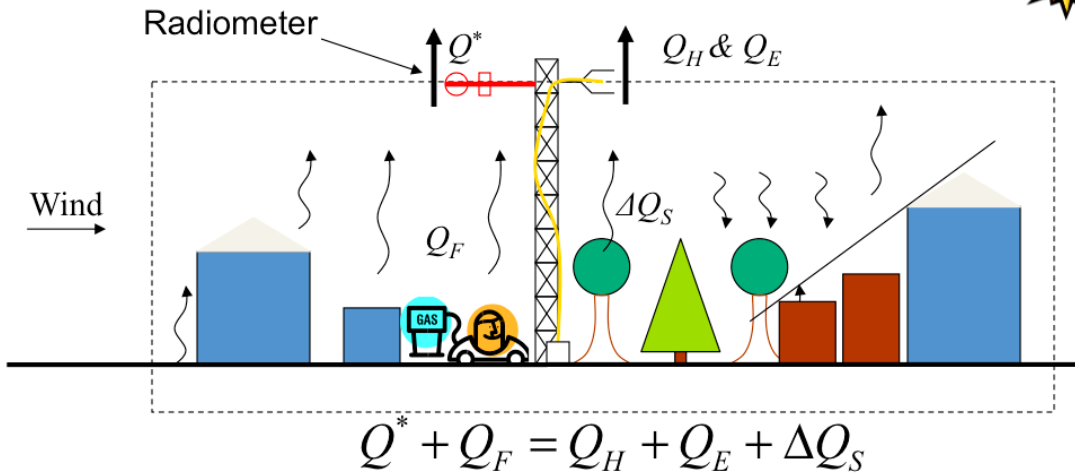
Joshua Hrisko^{1,3}, Prathap Ramamurthy^{1,3}, Jorge E. Gonzalez^{1,3}, Hamidreza Norouzi², Abdou Bah²

¹*City College of New York, New York, NY*

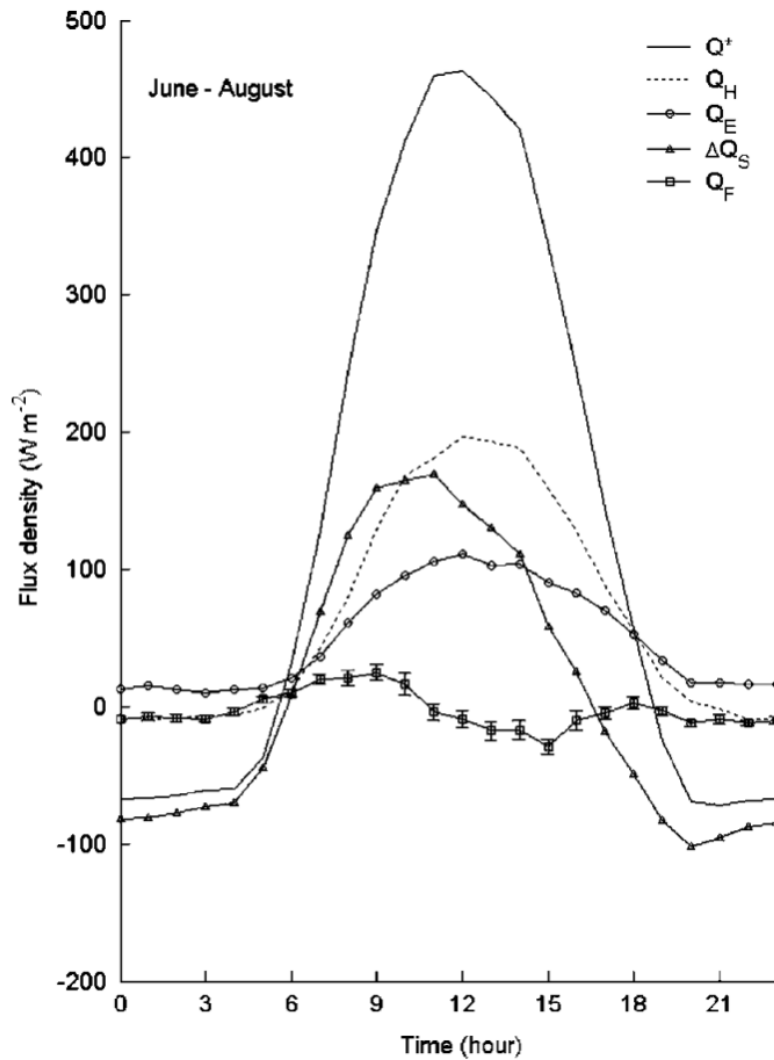
²*New York City College of Technology, Brooklyn, NY*

³*NOAA-CESSRST, New York, NY*

Urban Surface Energy Balance

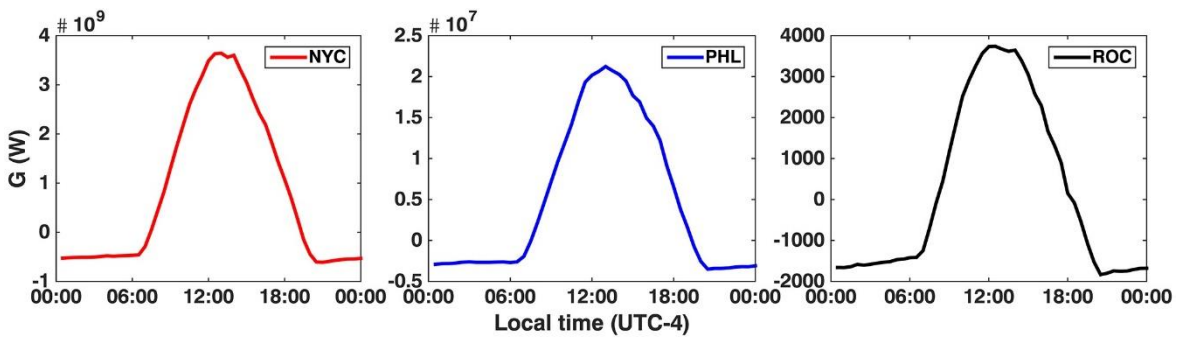


- Heat storage in urban areas is a significant term in the urban surface energy budget

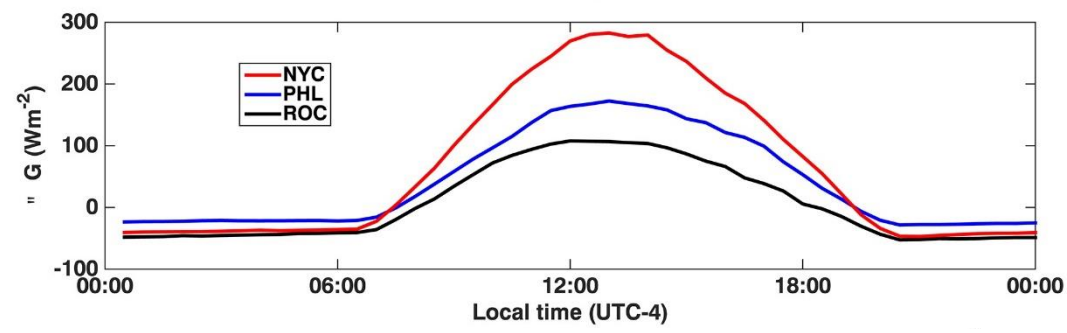


- Heat storage in urban areas is a significant term in the urban surface energy budget

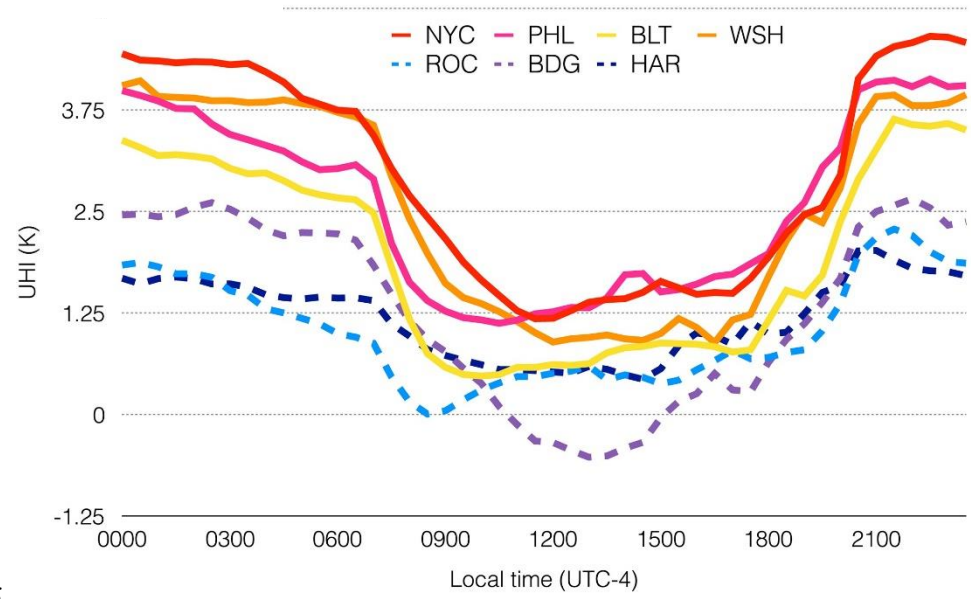
Offerle, B., Grimmond, C.S.B. and Fortuniak, K. (2005), Heat storage and anthropogenic heat flux in relation to the energy balance of a central European city centre. *Int. J. Climatol.*, 25: 1405-1419.



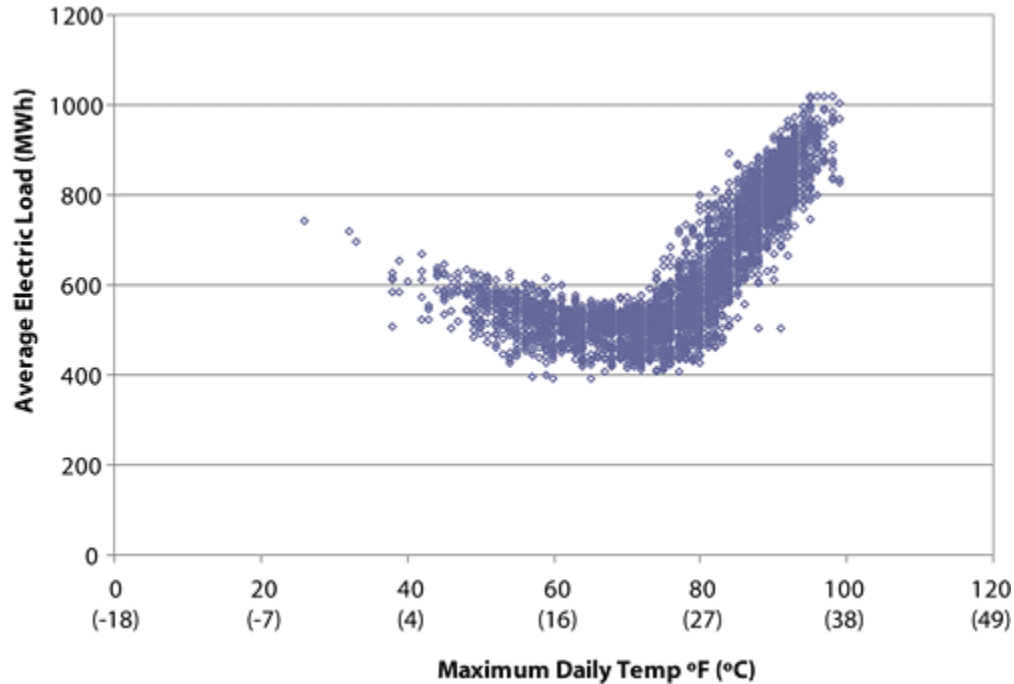
• UHI and heat storage are inextricably linked



“...this overwhelming disparity in storage heat flux is the primary factor that controls the daily pattern of UHI among cities”

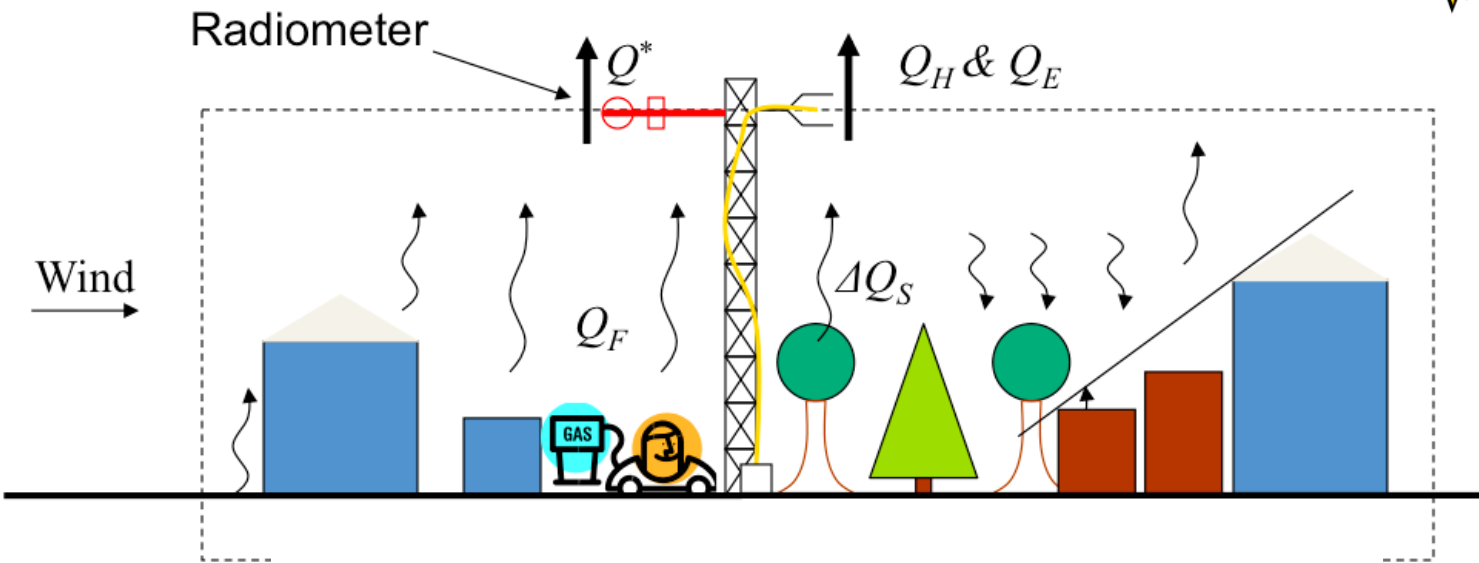


Ramamurthy, P., and Bou-Zeid, E. (2017), Heatwaves and urban heat islands: A comparative analysis of multiple cities, *J. Geophys. Res. Atmos.*, 122, 168- 178.



- Heat storage can also be used to approximate sensible heat fluxes, which can help predict air temperatures – ultimately relating to electric loads

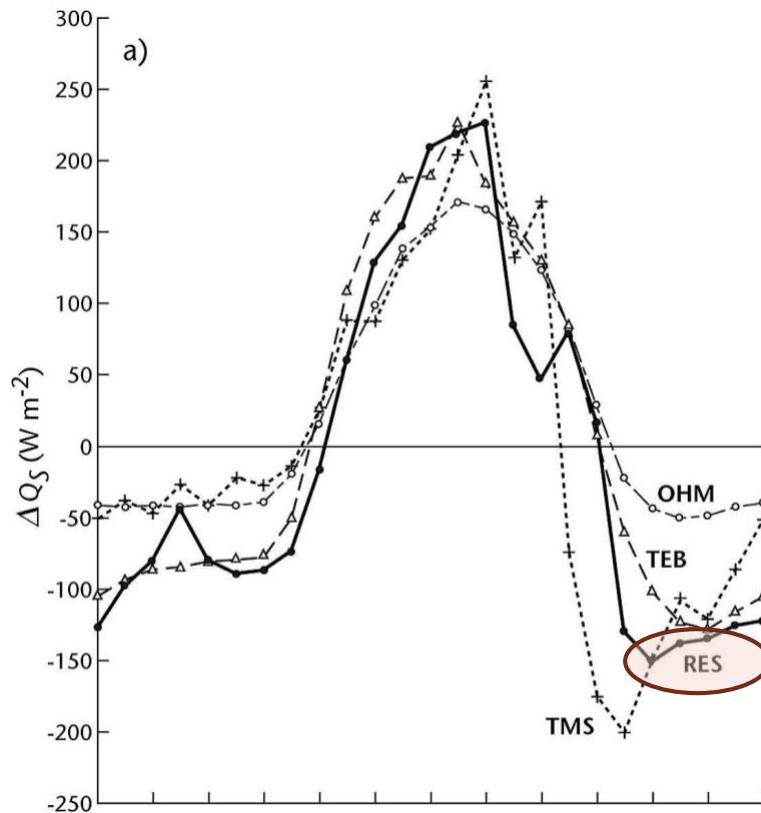
Urban Surface Energy Balance



$$\Delta Q_S = (Q^* + Q_F) - (Q_H + Q_{LE})$$



Previous Work



$$\Delta Q_S = (Q^* + Q_F) - (Q_H + Q_{LE})$$

ΔQ_S \equiv Heat storage [W · m⁻²]

Q^* \equiv Net radiation [W · m⁻²]

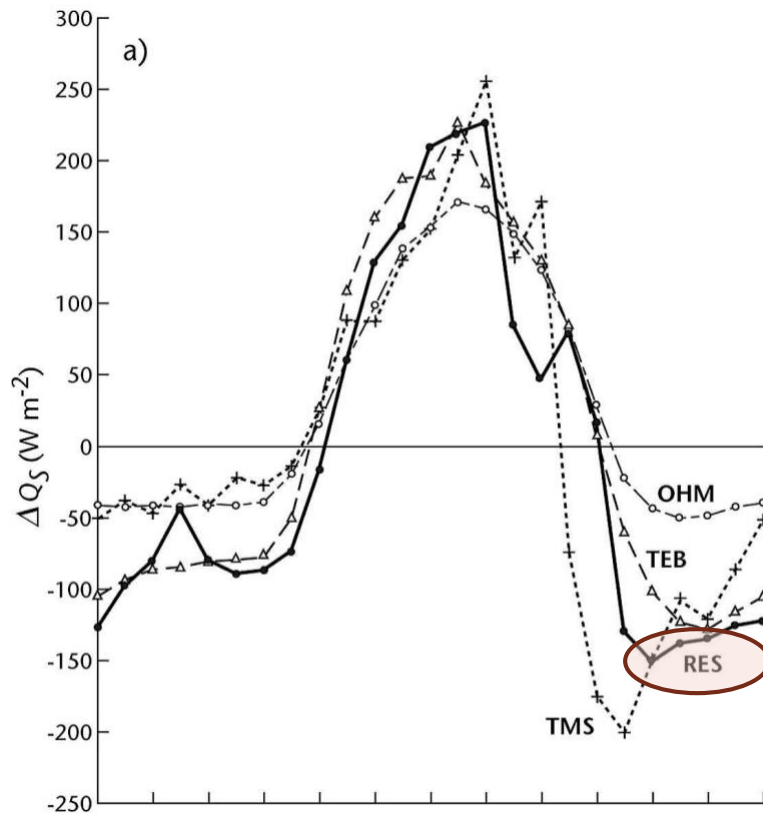
Q_F \equiv Anthropogenic Heat [W · m⁻²]

Q_H \equiv Sensible Heat [W · m⁻²]

Q_{LE} \equiv Latent Heat [W · m⁻²]



Previous Work

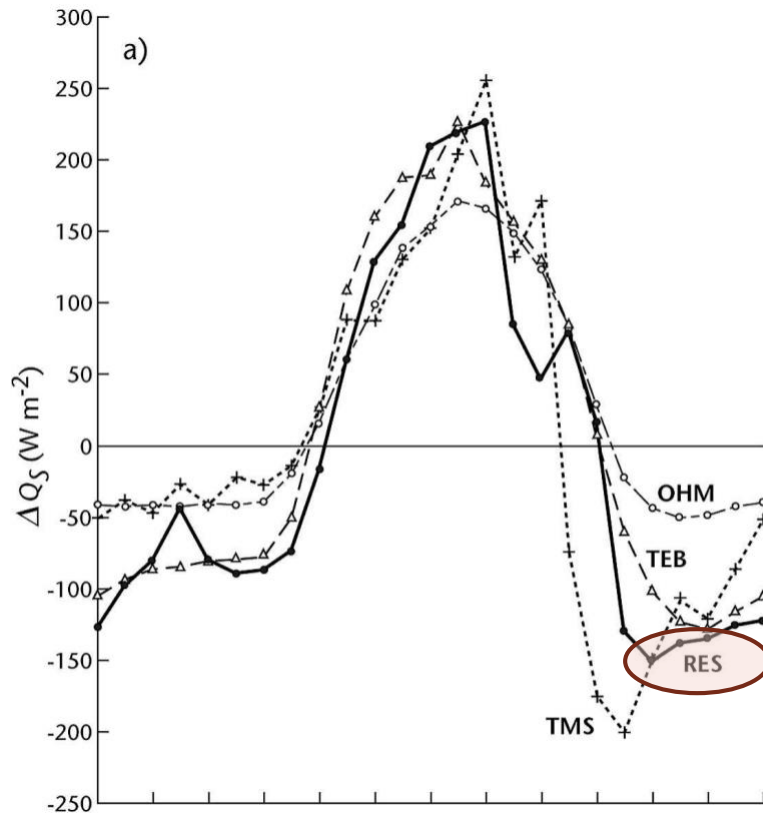


$$\Delta Q_S = (Q^* + Q_F) - (Q_H + Q_{LE})$$



“The instruments used to measure Q^* , Q_H , and Q_{LE} are expected to sense most of the Q_F contributions to the radiative and convective flux terms...” – therefore, Q_F is ignored here

Previous Work



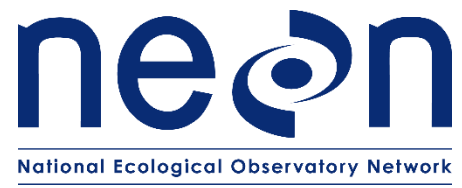
$$\Delta Q_s = (Q^* + Q_F) - (Q_H + Q_{LE})$$



“The instruments used to measure Q^* , Q_H , and Q_{LE} are expected to sense most of the Q_F contributions to the radiative and convective flux terms...” – therefore, Q_F is ignored here

$$\Delta Q_s = Q^* - (Q_H + Q_{LE})$$

Instrumentation



$$\Delta Q_s = Q^* - (Q_H + Q_{LE})$$

Component	Instrument
Q^*	Net Radiometer
Q_H	Sonic Anemometer + Gas Analyzer (H ₂ O)
Q_{LE}	



<http://www.nysmesonet.org/networks/flux>
<https://data.neonscience.org/data-product-view>

<https://www.kippzonen.com/Product/85/CNR4-Net-Radiometer>
<https://www.campbellsci.com/cpec200>

Instrumentation



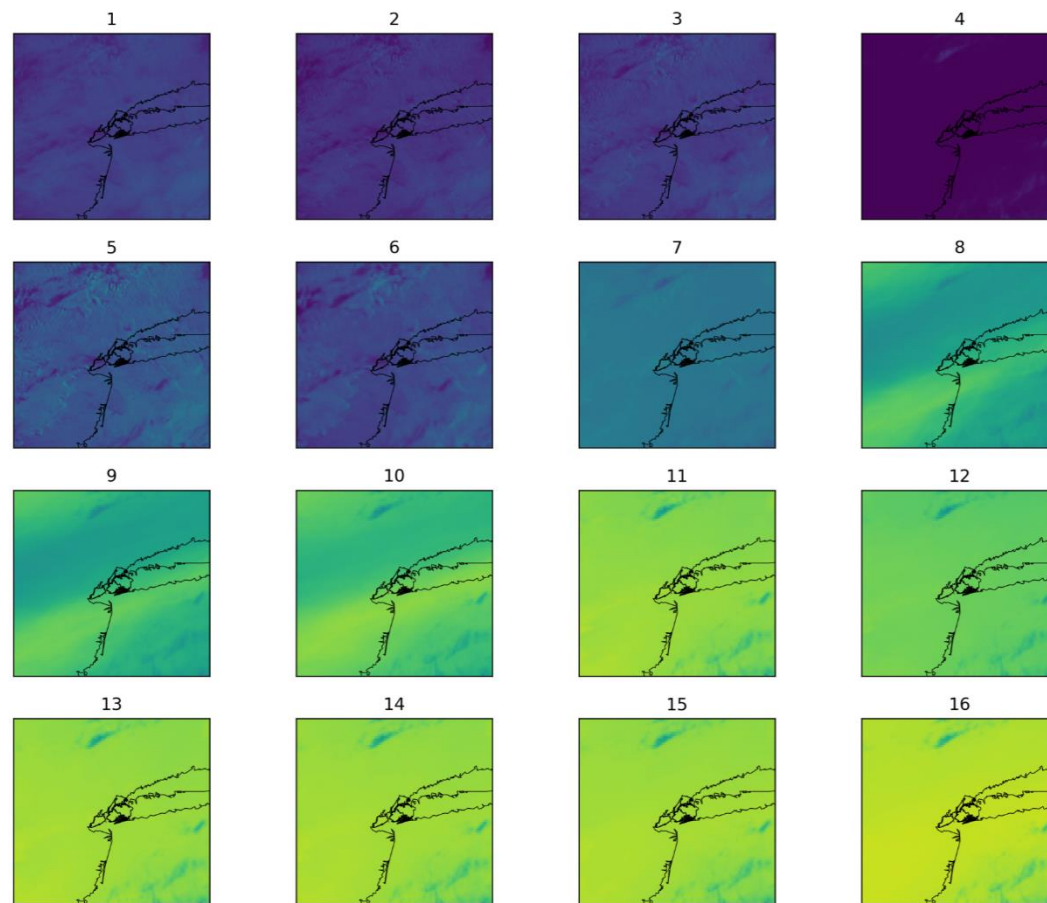
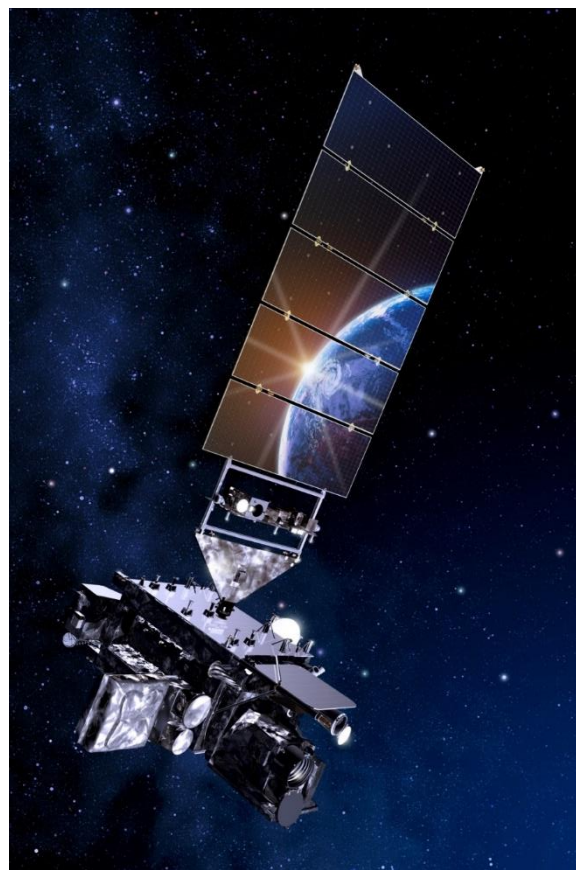
GOES-16 Satellite

- 5-min time resolution
- 0.5 km - 2.0 km spatial resolution
- Positioned over east coast in U.S. (75.2 W)

<https://www.nasa.gov/directorates/heo/scan/services/missions/earth/GOES16.html>

Instrumentation

Spectral radiance (L_λ) for each of the GOES-16 bands



Radiance [$\text{W} \cdot \text{m}^{-2} \text{sr}^{-1} \mu\text{m}^{-1}$]

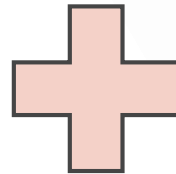
<https://www.nasa.gov/directorates/heo/scan/services/missions/earth/GOES16.html>

Hypothesis



$$\Delta Q_s = Q^* - (Q_H + Q_{LE})$$

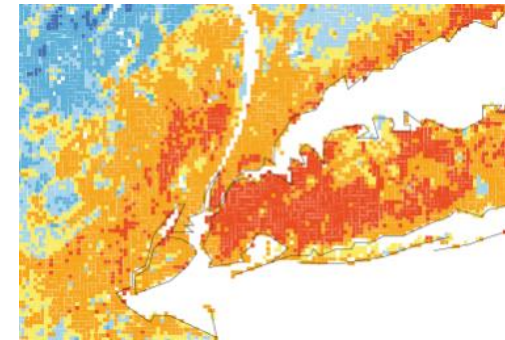
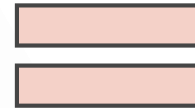
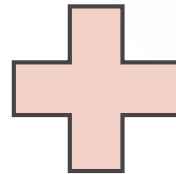
Hypothesis



$$\Delta Q_s = Q^* - (Q_H + Q_{LE})$$

$$L_{\lambda_1 - \lambda_{16}}$$

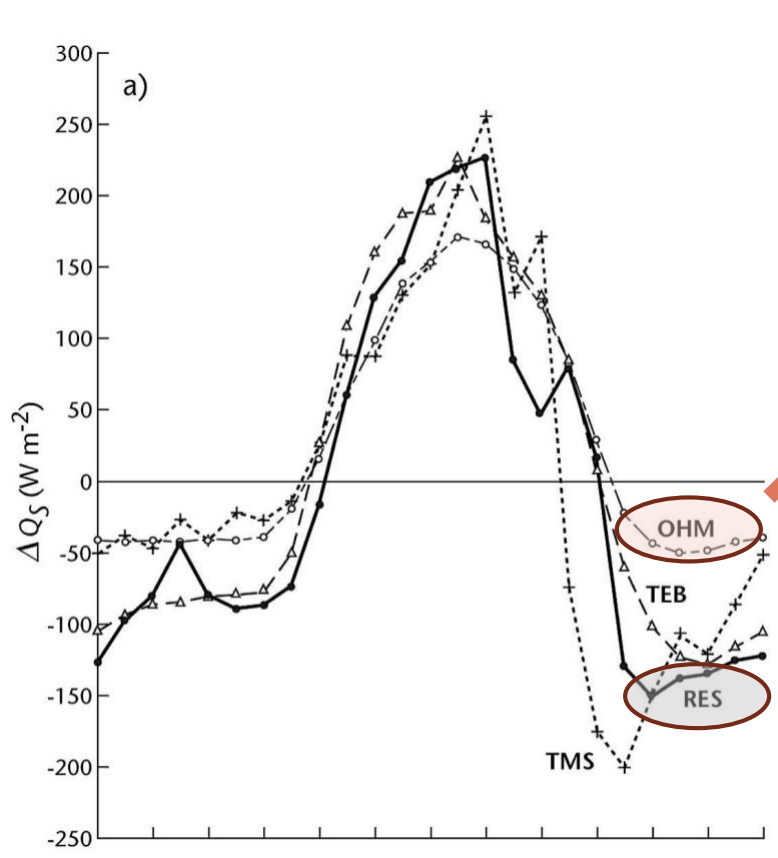
Hypothesis



$$\Delta Q_s = Q^* - (Q_H + Q_{LE})$$

$$\Delta Q_s$$
$$L\lambda_1 - \lambda_{16}$$

Hypothesis



Objective Hysteresis Model

$$\Delta Q_s = a_1 Q^* + a_2 \frac{\partial Q^*}{\partial t} + a_3$$

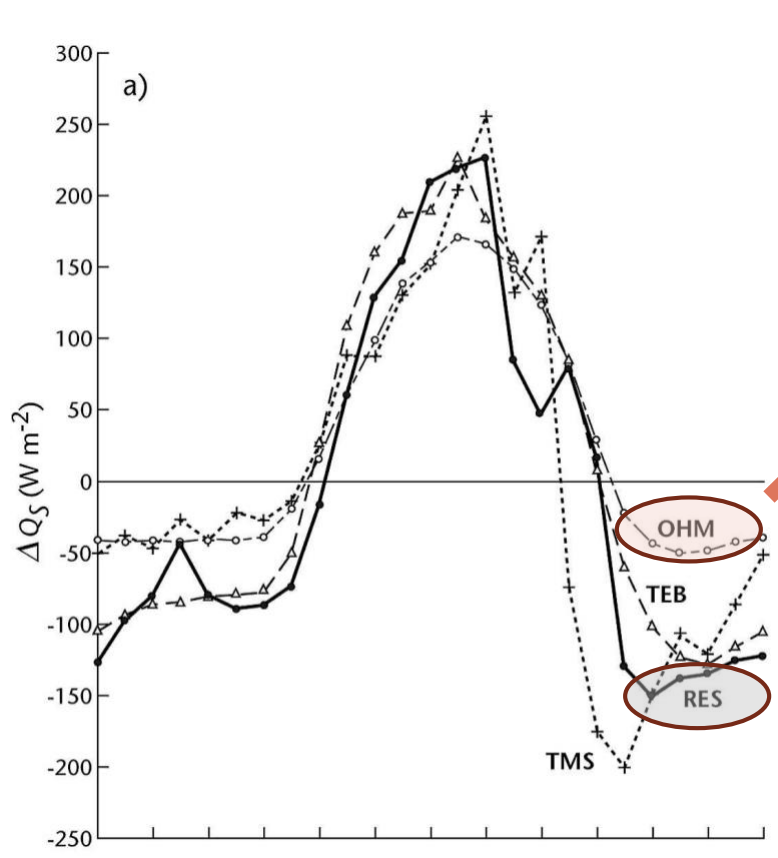


ΔQ_s

Roberts, S.M., T.R. Oke, C.S. Grimmond, and J.A.Voogt, 2006: Comparison of Four Methods to Estimate Urban Heat Storage. *J. Appl. Meteor. Climatol.*, **45**, 1766–1781.

$L_{\lambda_1-\lambda_{16}}$

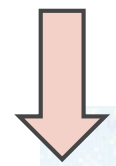
Hypothesis



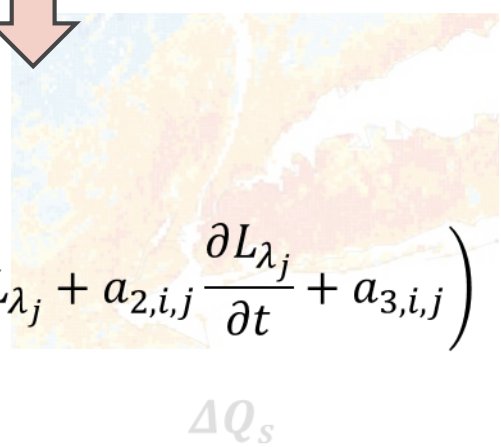
Roberts, S.M., T.R. Oke, C.S. Grimmond, and J.A.Voogt, 2006: Comparison of Four Methods to Estimate Urban Heat Storage. *J. Appl. Meteor. Climatol.*, **45**, 1766–1781.

Objective Hysteresis Model

$$\Delta Q_s = a_1 Q^* + a_2 \frac{\partial Q^*}{\partial t} + a_3$$



$$\Delta Q_s = \sum_i \sum_j \left(a_{1,i,j} L_{\lambda_j} + a_{2,i,j} \frac{\partial L_{\lambda_j}}{\partial t} + a_{3,i,j} \right)$$

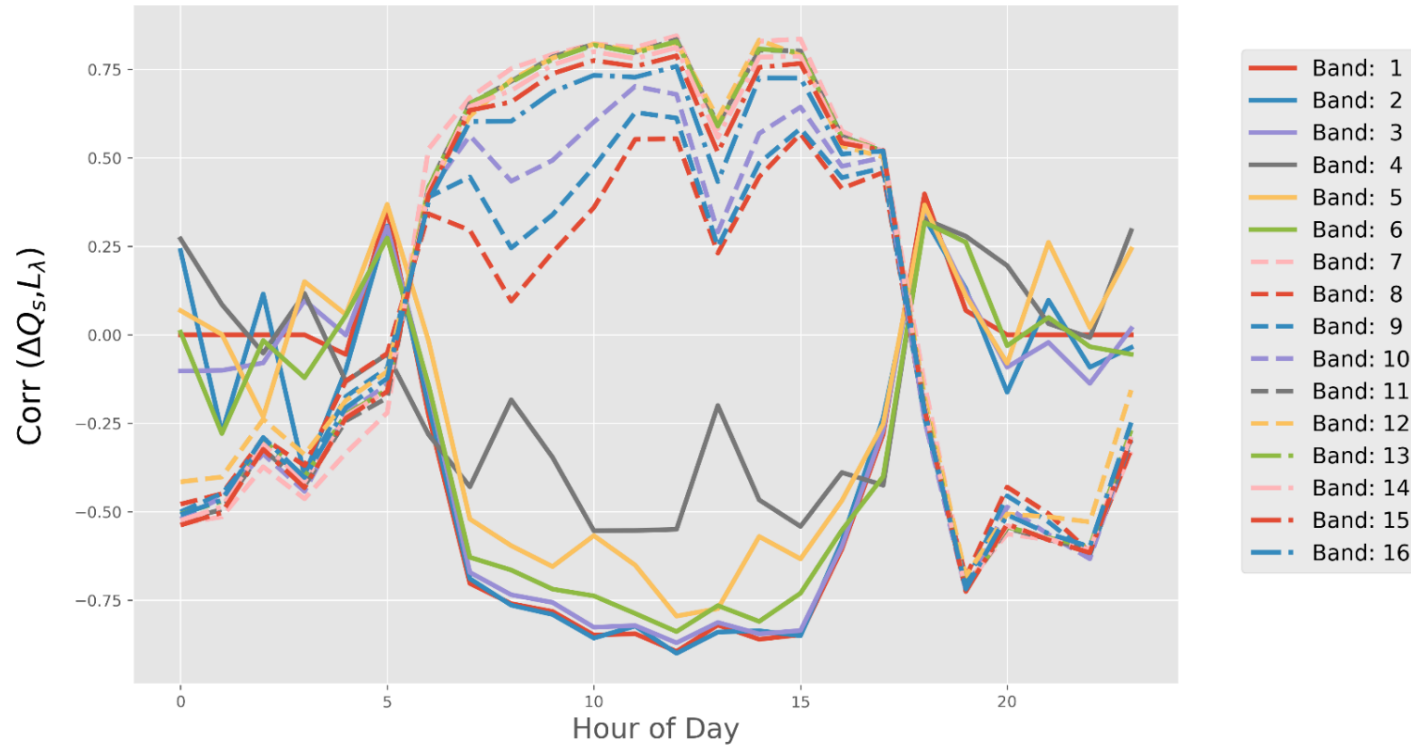


$a_1, a_2, a_3 \equiv$ coefficients

$L_{\lambda_1 - \lambda_{16}}$



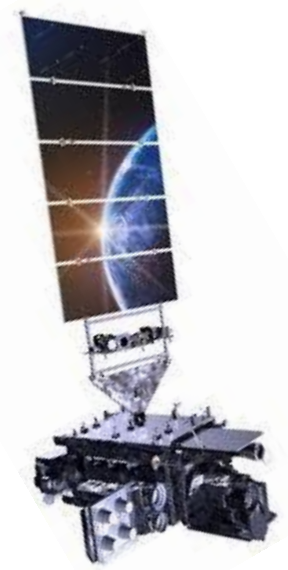
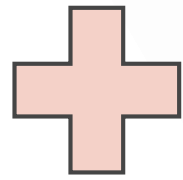
Hypothesis



All stations exhibit similar correlative behavior over GOES-16 bands and local time

$$\text{Corr} \equiv \frac{\text{cov}(x,y)}{\sigma_x \sigma_y} = \frac{\sum_i (x_i - \bar{x}) \cdot (y_i - \bar{y})}{\sqrt{\sum_i (x_i - \bar{x})^2} \cdot \sqrt{\sum_i (y_i - \bar{y})^2}}$$

Implementation



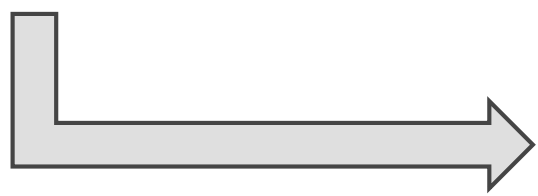
$L_{\lambda_1-\lambda_{16}}$

$$\Delta Q_s = Q^* - (Q_H + Q_{LE})$$

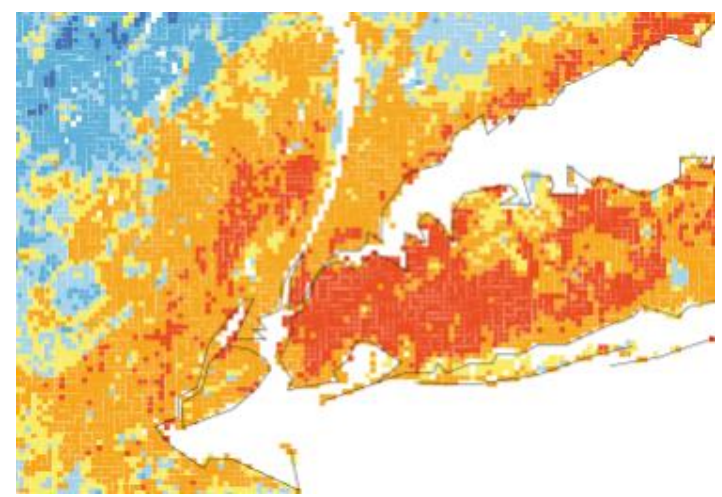
training

$$\Delta Q_s \propto L_{\lambda,j}$$

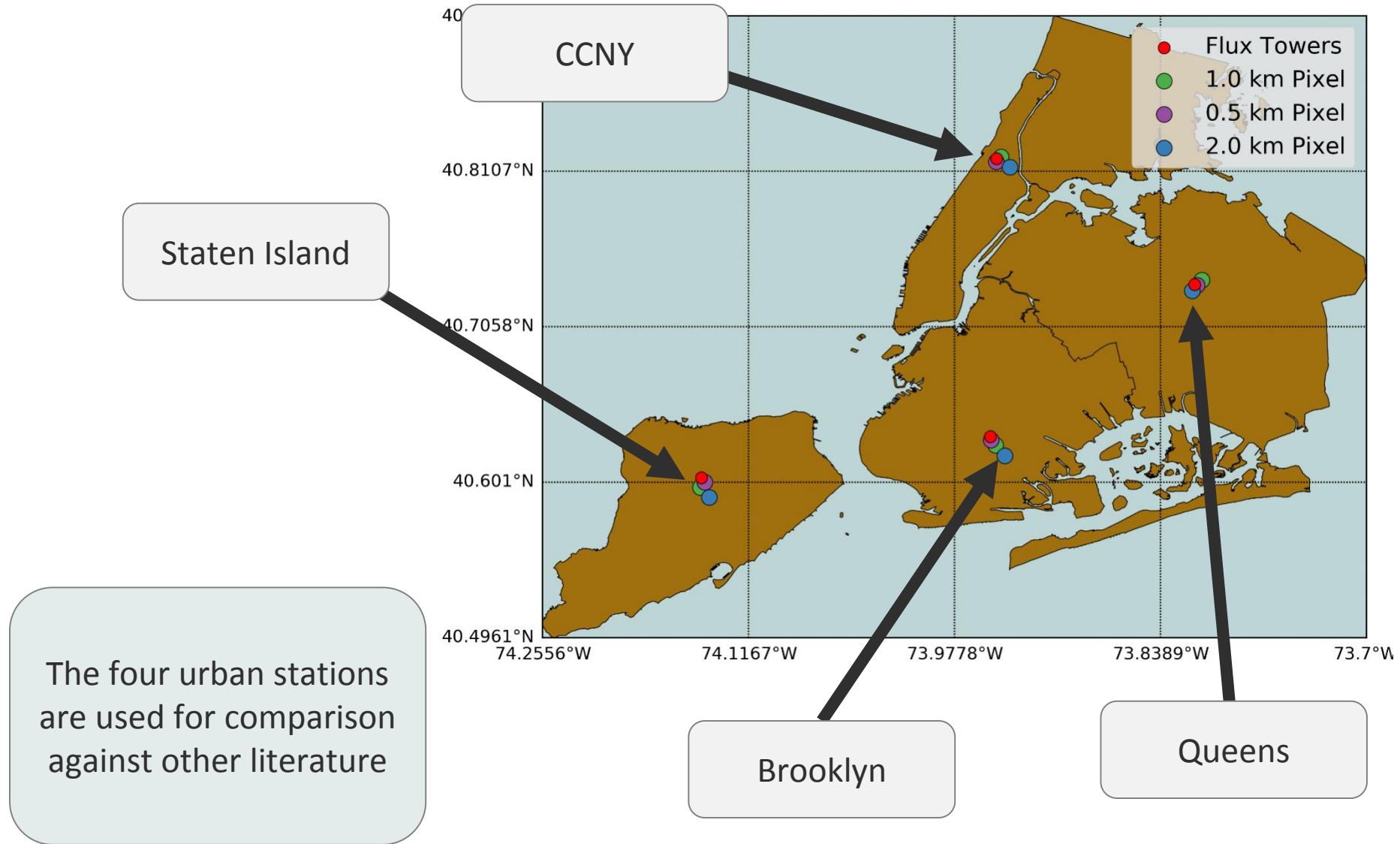
$$\Delta Q_s = \sum_i \sum_j \left(a_{1,i,j} L_{\lambda_j} + a_{2,i,j} \frac{\partial L_{\lambda_j}}{\partial t} + a_{3,i,j} \right)$$



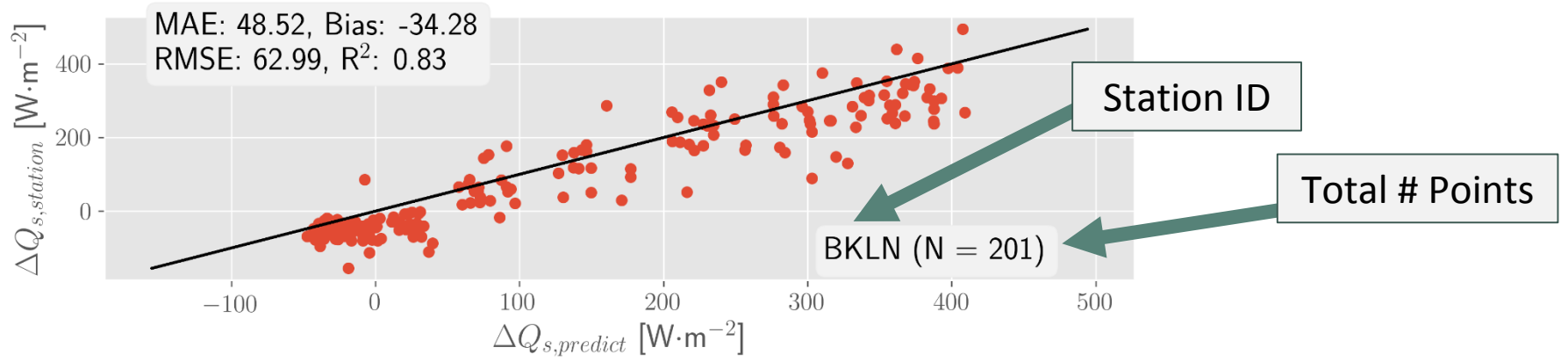
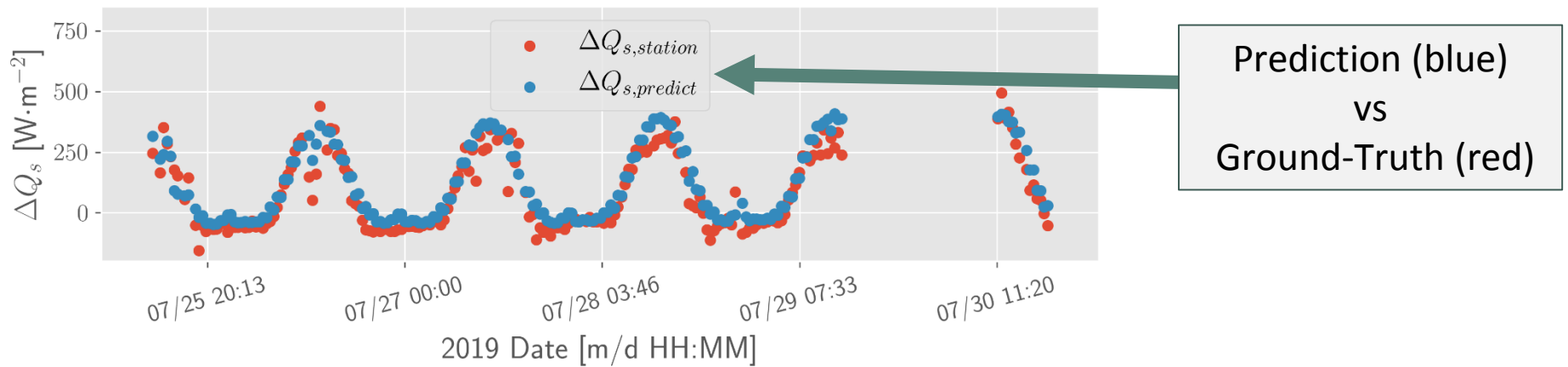
ΔQ_s



Analysis Locations



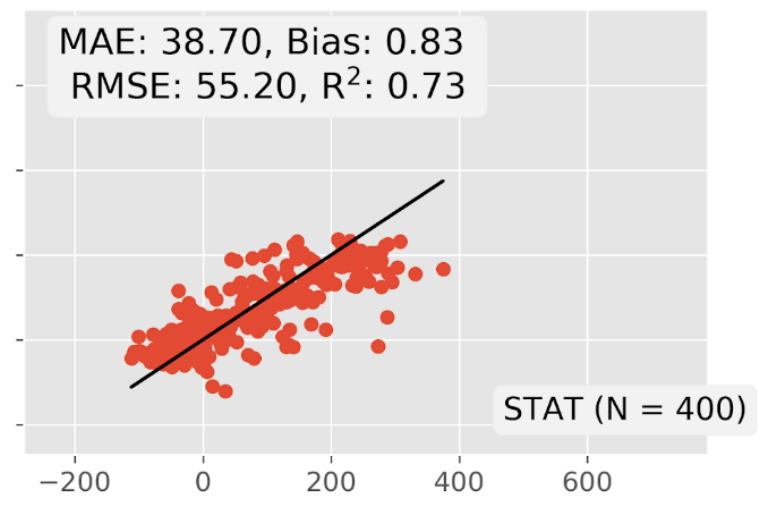
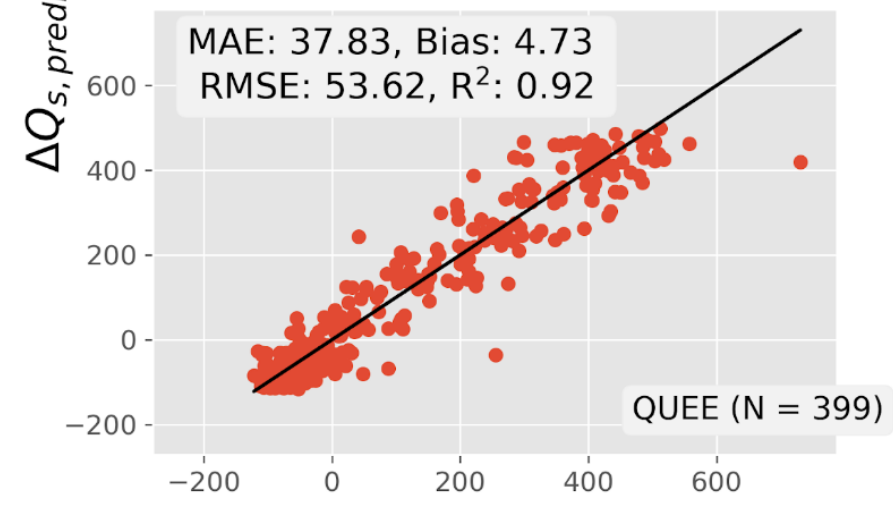
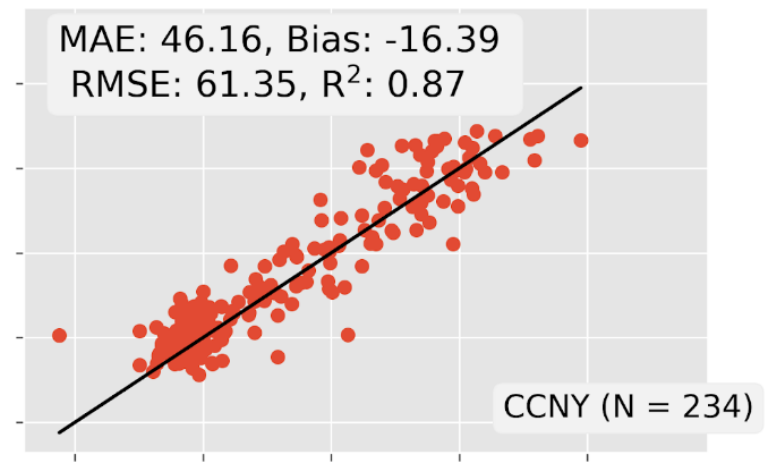
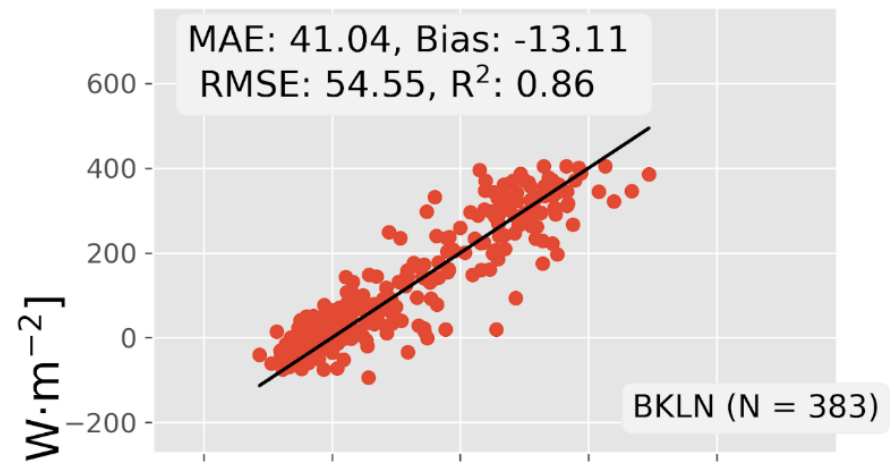
Analysis Metrics



$MAE = \frac{1}{n} \sum_{i=1}^n \Delta Q_{s,station} - \Delta Q_{s,predict} $	$RMSE = \sqrt{\frac{1}{n} \sum_{i=1}^n (\Delta Q_{s,station} - \Delta Q_{s,predict})^2}$
$Bias = \frac{1}{n} \sum_{i=1}^n (\Delta Q_{s,station} - \Delta Q_{s,predict})$	$R^2 = 1 - \frac{SS_{res}}{SS_{tot}} = 1 - \frac{\sum_i (\Delta Q_{s,station} - \Delta Q_{s,predict})^2}{\sum_i (\Delta Q_{s,station} - \overline{\Delta Q_{s,station}})^2}$

70% Data Training using multivariate linear regression and non-linear temporal spline

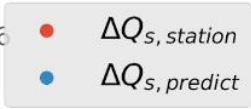
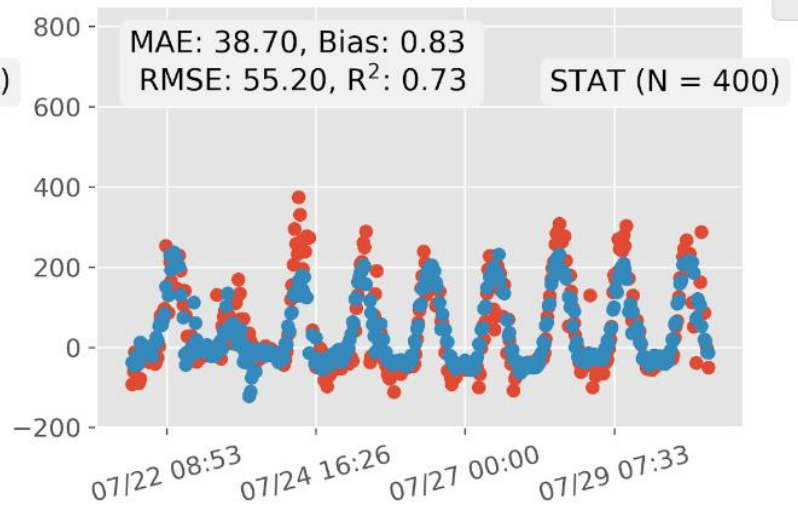
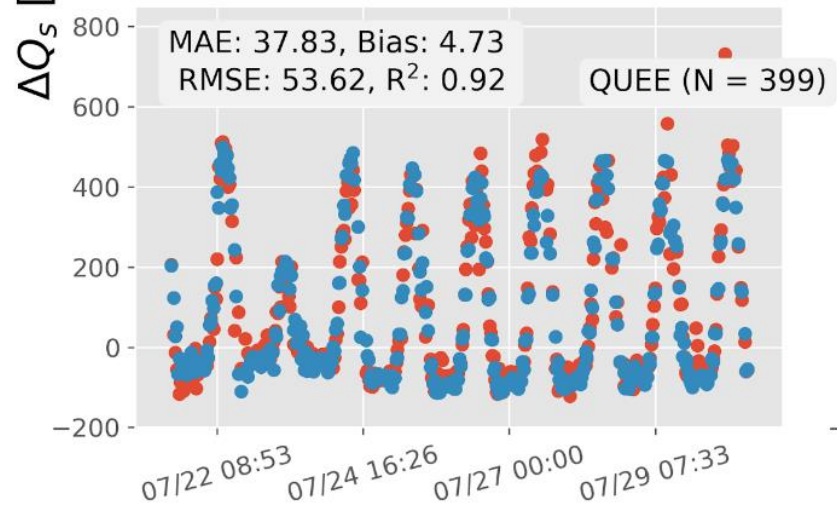
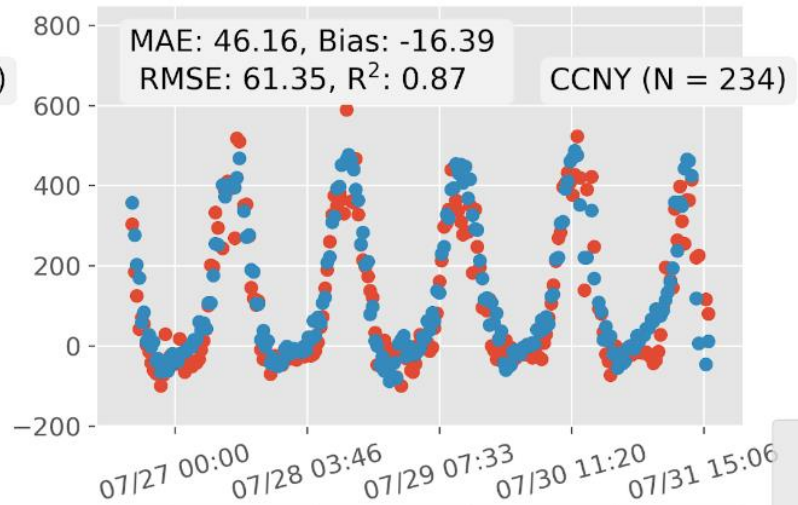
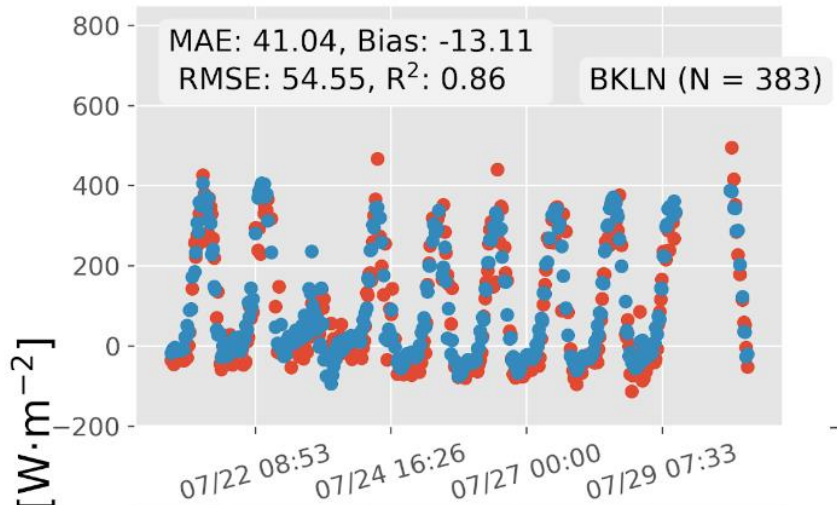
Validation Plots



$\Delta Q_{s,station} [W \cdot m^{-2}]$

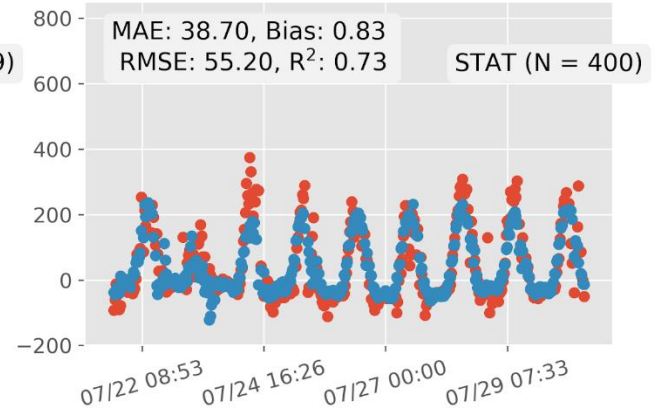
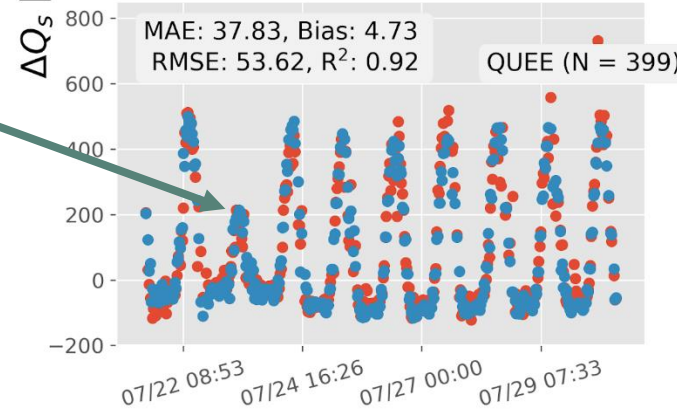
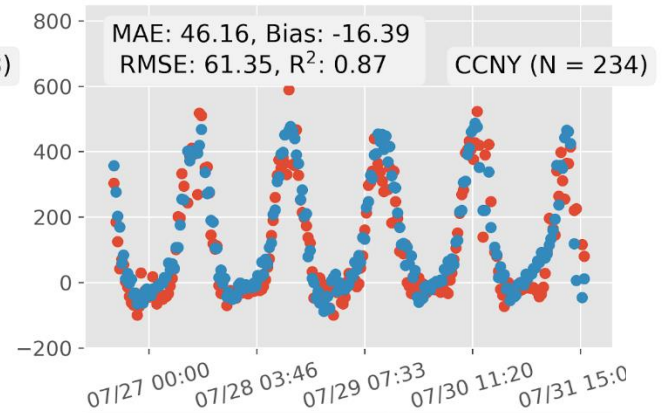
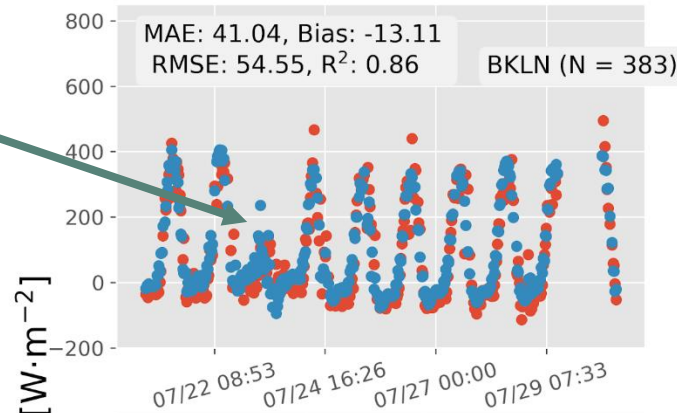
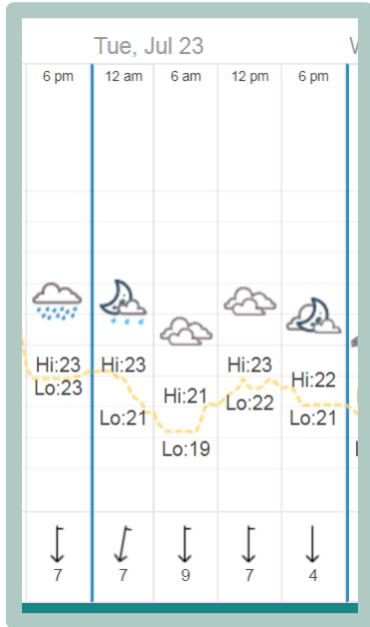
70% Data Training using multivariate linear regression and non-linear temporal spline

Validation Plots



Date in 2019 [m/d HH:MM]

Validation Plots



Date in 2019 [m/d HH:MM]

Our 16-band algorithm performs fairly well, even under rainy/cloudy conditions – robust for a satellite algorithm!

Literature Comparison

Site/description	<i>N</i>	Slope	Intercept (W m^{-2})	r^2	Rmse (W m^{-2})
Los Angeles, California (residential suburb)	424	0.97	4.0	0.92	29.0
Mexico City (city center)	61	0.89	-6.8	0.96	33.6
Vancouver (light industrial)	312	0.96	-4.5	0.88	48.9
Miami, Florida (residential suburb)	204	0.98	22.9	0.79	61.9
Suburban Vancouver	464	0.75	30.8	0.67	62.9
Sacramento, California (residential suburb)	222	0.55	5.0	0.56	66.0
Chicago, Illinois (residential suburb)	163	0.81	38.8	0.56	83.3
Marseille (city center)	192	0.49	31.0	0.70	94.8
Tucson (residential suburb)	75	1.21	66.1	0.75	107.4

Site	<i>N</i>	R^2	RMSE
Brooklyn (100% Urban)	383	0.86	54.6
CCNY (91% Urban)	234	0.87	61.4
Queens (99% Urban)	399	0.92	53.6
Staten Island (57% Urban)	400	0.73	55.2

Roberts, S.M., T.R. Oke, C.S. Grimmond, and J.A.Voogt, 2006: Comparison of Four Methods to Estimate Urban Heat Storage. *J. Appl. Meteor. Climatol.*, **45**, 1766–1781.

Literature Comparison

Site/description	N	Slope	Intercept (W m^{-2})	r^2	Rmse (W m^{-2})
Los Angeles, California (residential suburb)	424	0.97	4.0	0.92	29.0
Mexico City (city center)	61	0.89	-6.8	0.96	33.6
Vancouver (light industrial)	312	0.95	-4.5	0.88	48.9
Miami, Florida (residential suburb)	284	0.78	11.2	0.79	61.9
Suburban Vancouver	464	0.75	30.8	0.67	62.9
Sacramento, California (residential suburb)	222	0.55	5.0	0.56	66.0
Chicago, Illinois (residential suburb)	163	0.81	38.8	0.56	83.3
Marseille (city center)	192	0.49	31.0	0.70	94.8
Tucson (residential suburb)	75	1.21	66.1	0.75	107.4

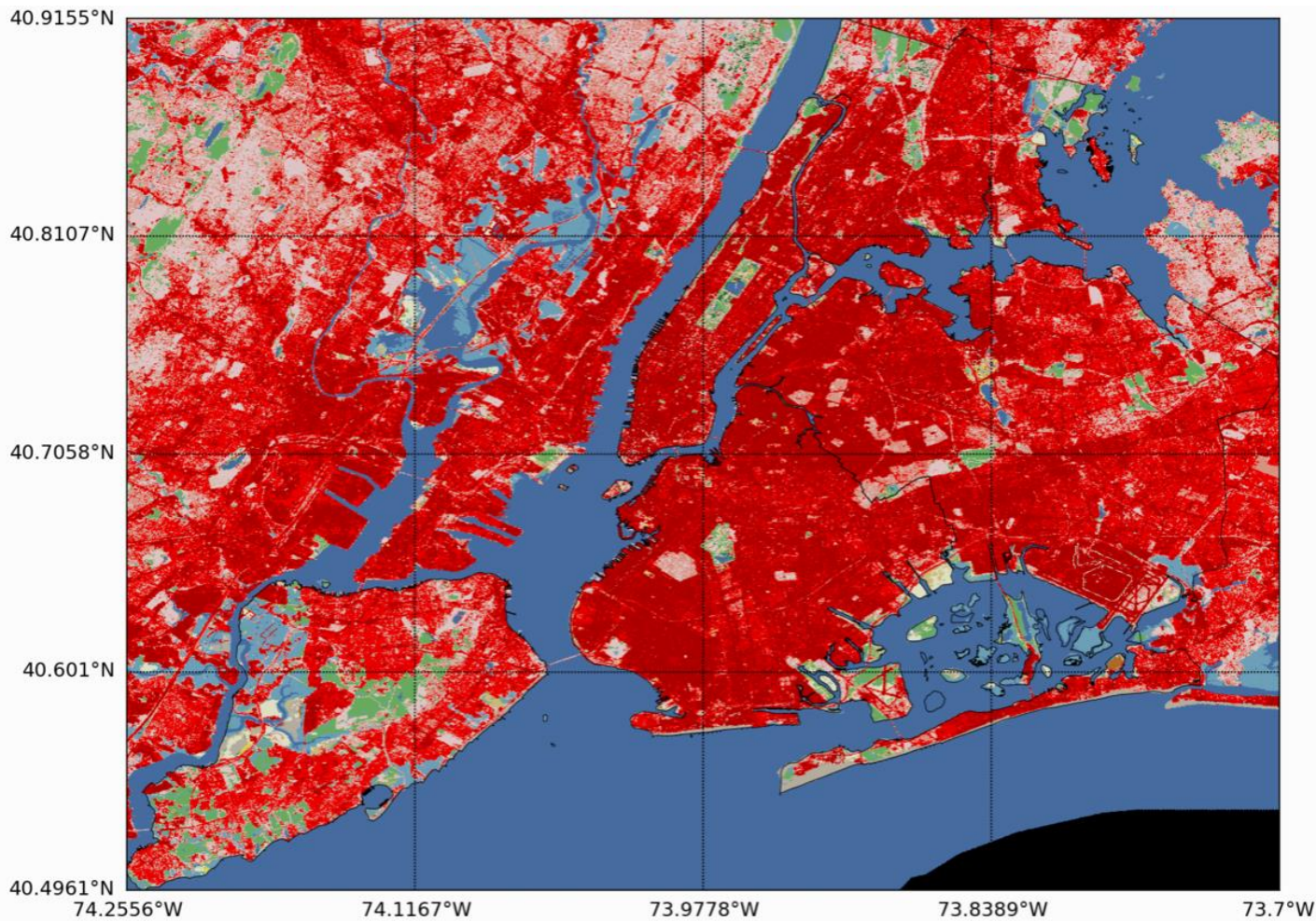
OHM average RMSE in literature: 65.3 [$\text{W} \cdot \text{m}^{-2}$]

Site	N		
Brooklyn (100% Urban)	335		0.83
CCNY (91% Urban)	200		0.83
Queens (99% Urban)	347		0.90
Staten Island (57% Urban)	350		0.73

Satellite algorithm average RMSE: 56.2 [$\text{W} \cdot \text{m}^{-2}$]



Spatial Reconstructions



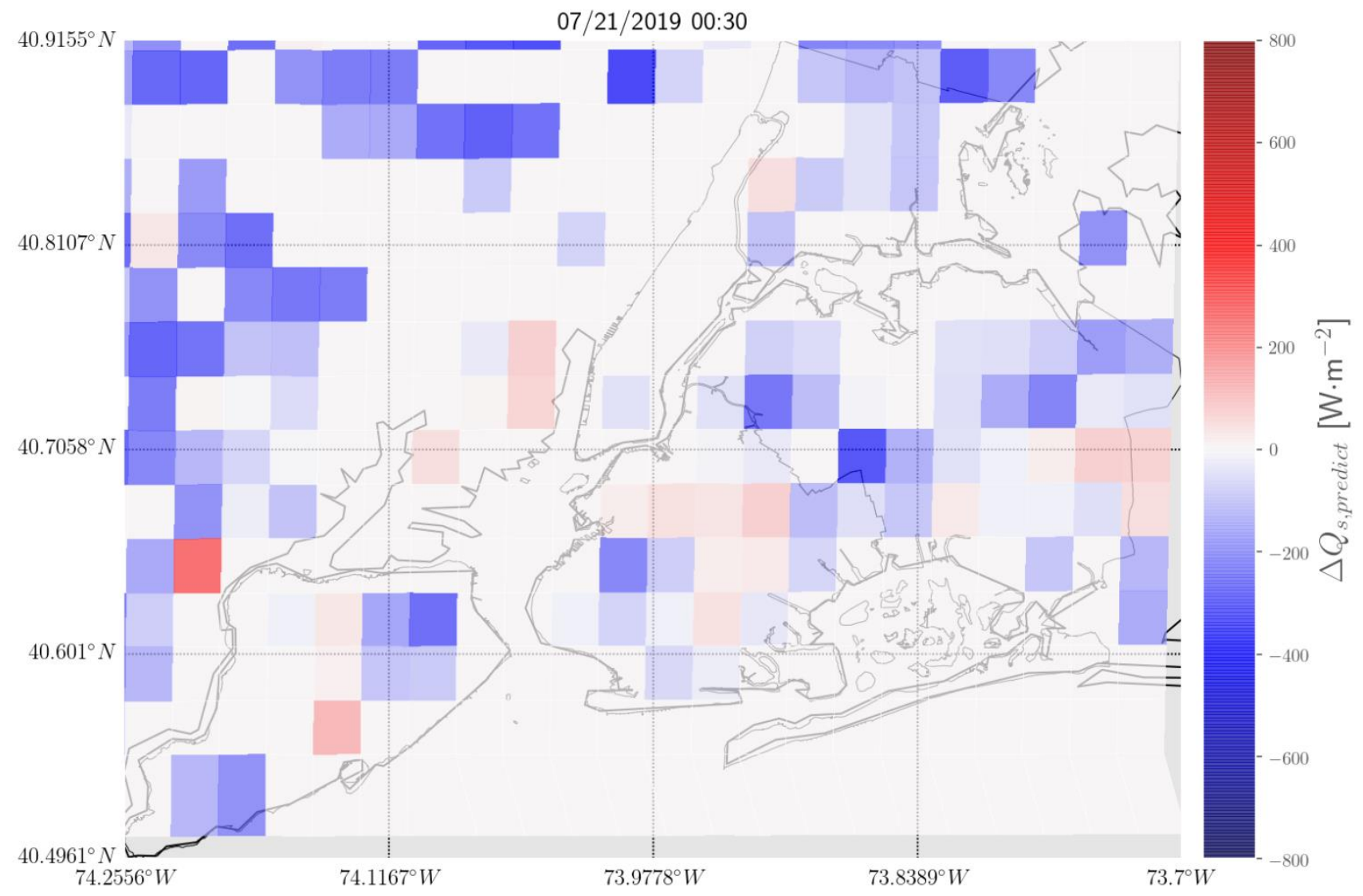
NLCD Land Cover Classification Legend

11	Open Water
12	Perennial Ice/ Snow
21	Developed, Open Space
22	Developed, Low Intensity
23	Developed, Medium Intensity
24	Developed, High Intensity
31	Barren Land (Rock/Sand/Clay)
41	Deciduous Forest
42	Evergreen Forest
43	Mixed Forest
51	Dwarf Scrub*
52	Shrub/Scrub
71	Grassland/Herbaceous
72	Sedge/Herbaceous*
73	Lichens*
74	Moss*
81	Pasture/Hay
82	Cultivated Crops
90	Woody Wetlands
95	Emergent Herbaceous Wetlands

* Alaska only

Spatial Reconstructions

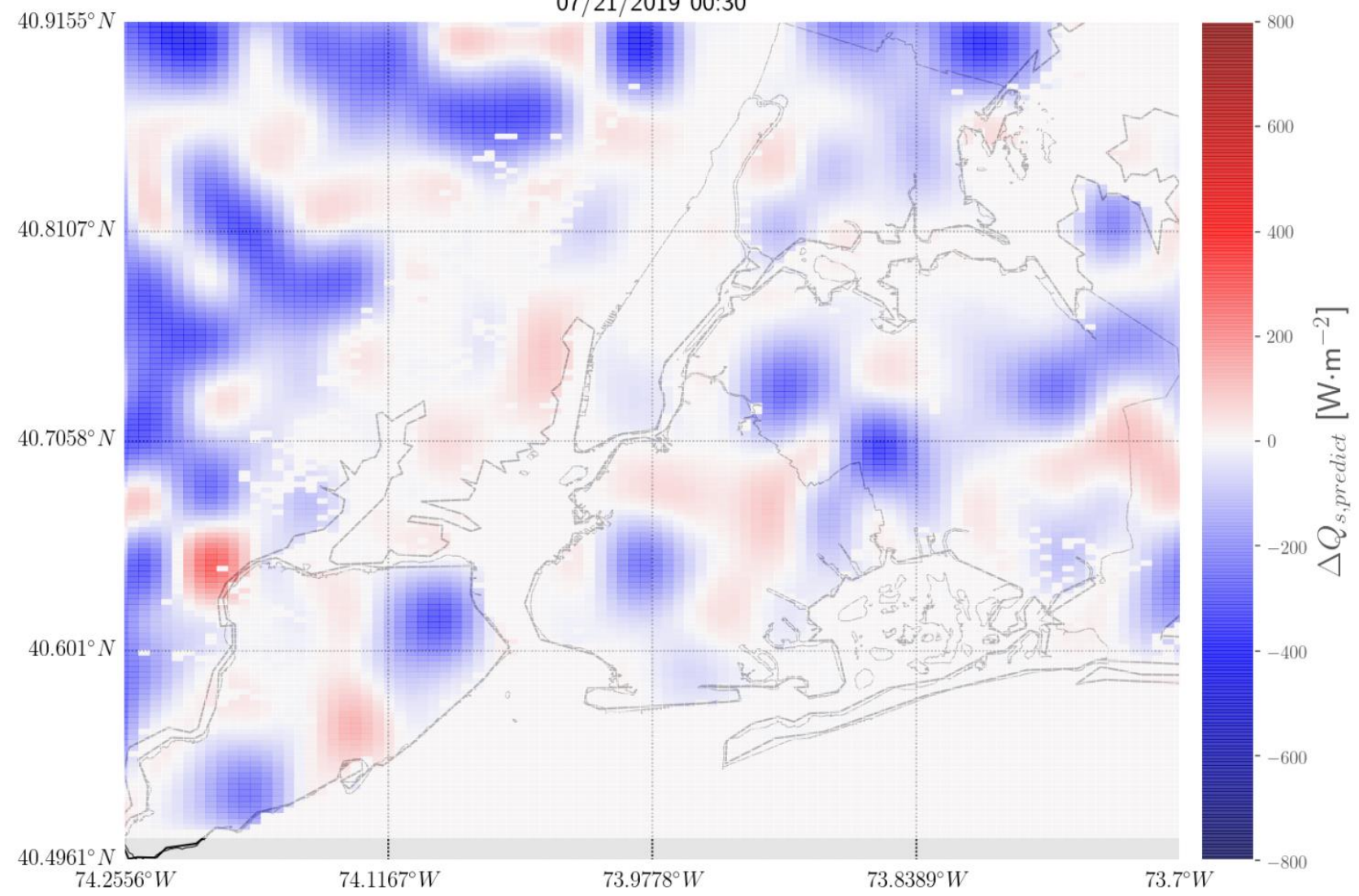
Native GOES-16 2km Resolution



Spatial Reconstructions

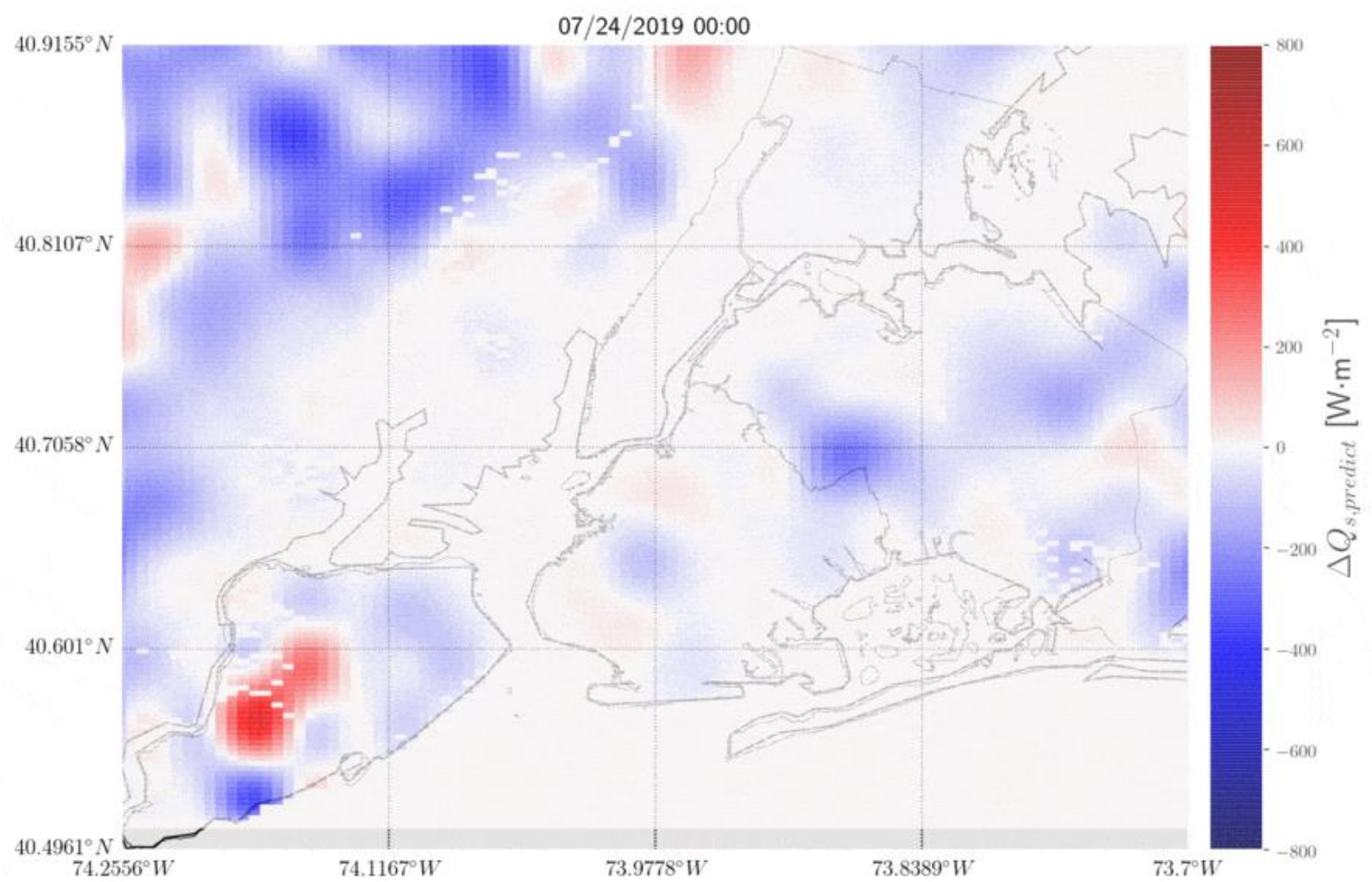
Bicubic Interpolation (320m Resolution)

07/21/2019 00:30



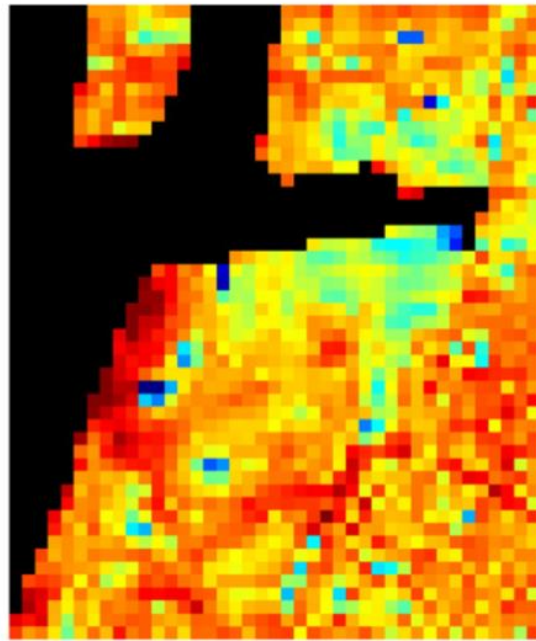
Spatial Reconstructions

Bicubic Interpolation (320m Resolution)

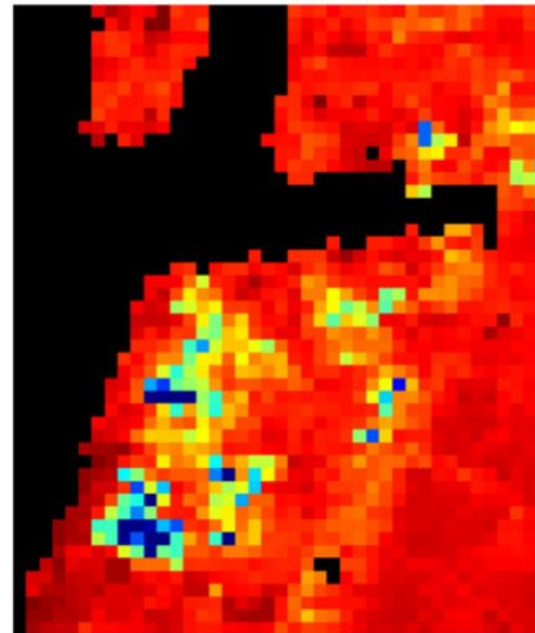


Literature Comparison

Storage heat flux in daytime on July 10, 2000



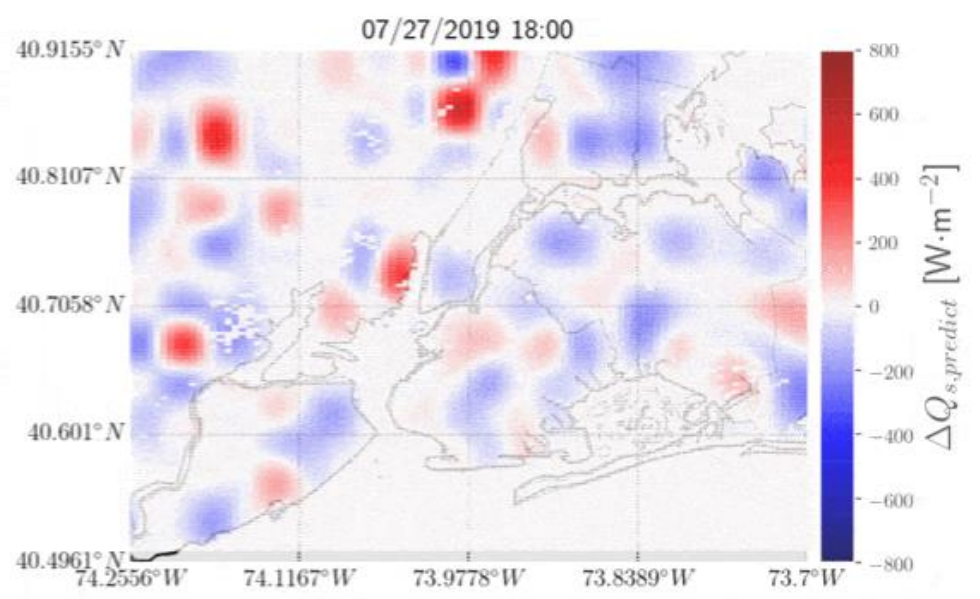
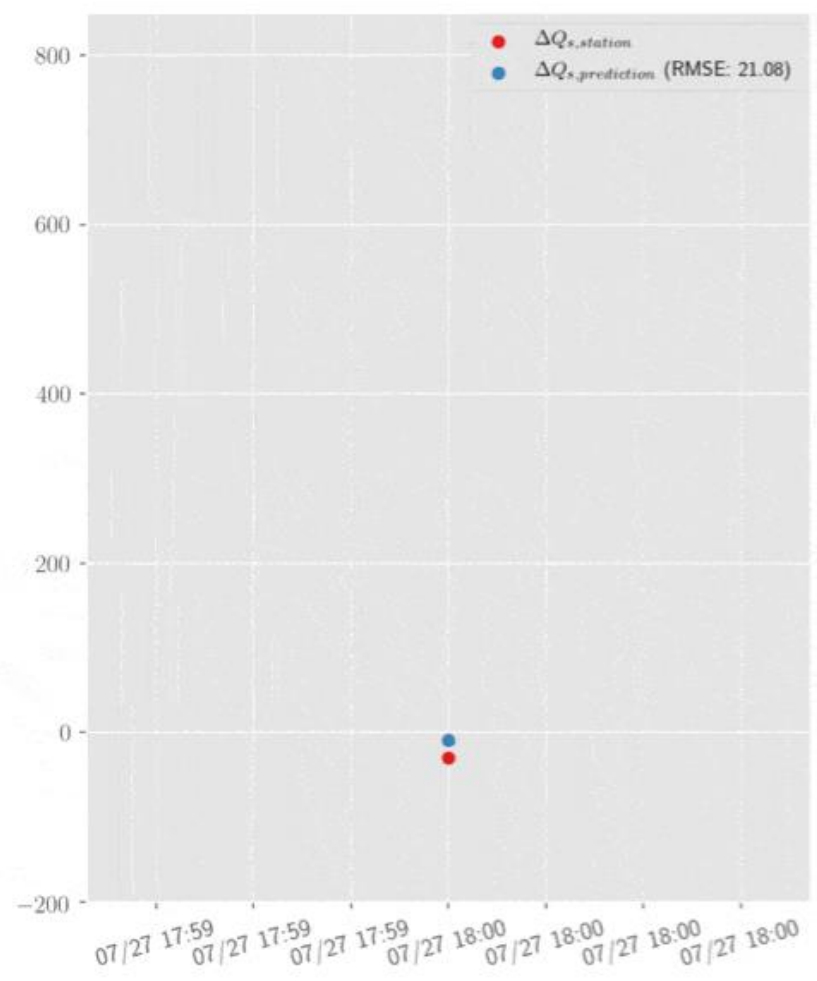
Storage heat flux at night on September 26, 2003



Similar spatial profiles for day and night in Nagoya, Japan

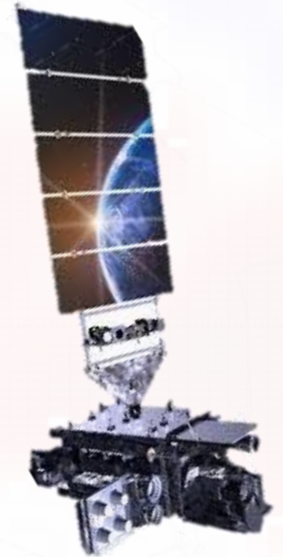
Interpolation Performance

Bicubic Interpolation (320m Resolution), comparison with QUEENS Station (independent verification), July 27th-29th, 90% training



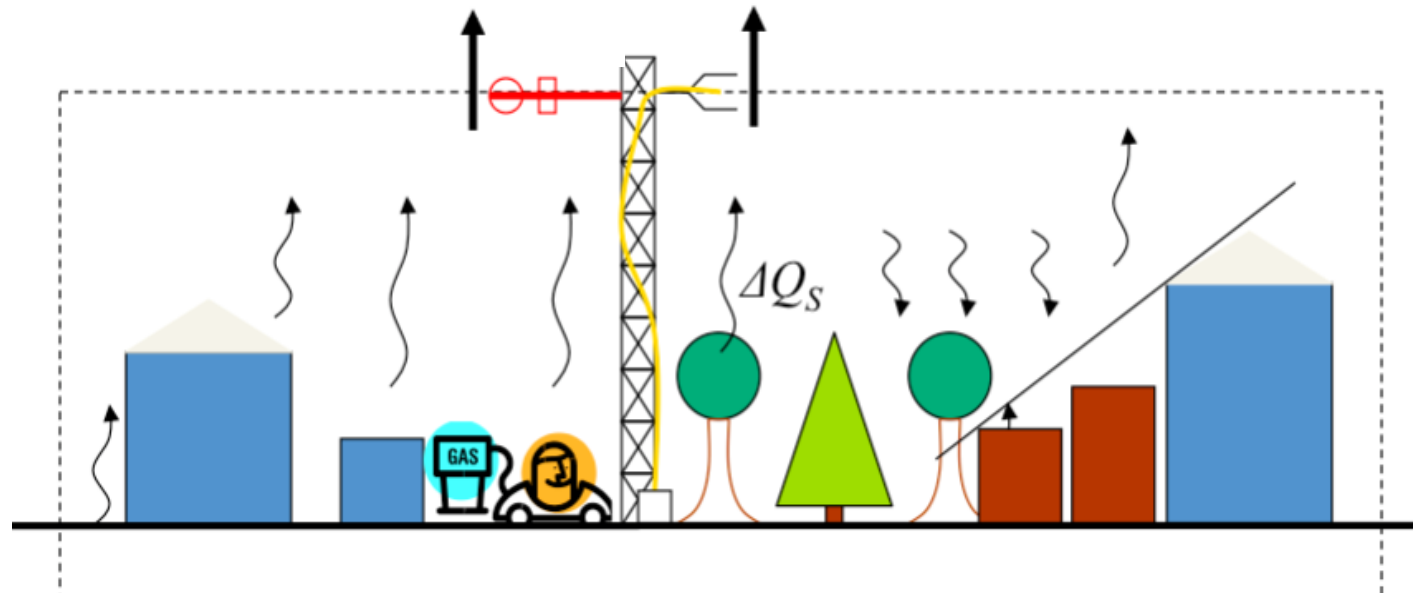
Key Takeaways:

1. The GOES-16 satellite Objective Hysteresis Model (OHM) is competitive with other storage calculation methods
2. The satellite OHM is able to capture the full diurnal cycle of heat storage
3. The spatial distribution of ΔQ_s is promising for calculation of a citywide heat storage product



Future Work:

- Thermal Mas Scheme (TMS) implementation using land cover
- Compare with urban numerical model



Acknowledgements

This study is supported and monitored by The National Oceanic and Atmospheric Administration – Cooperative Science Center for Earth System Sciences and Remote Sensing Technologies under the Cooperative Agreement Grant #: NA16SEC4810008. The authors would like to thank The City College of New York and NOAA Office of Education, Educational Partnership Program with Minority Serving Institutions (EPP/MSI) for full fellowship support for Joshua Hrisko. The statements contained within the manuscript/research article are not the opinions of the funding agency or the U.S. government, but reflect the author's opinions. This research is also made possible by the New York State (NYS) Mesonet. Original funding for the NYS Mesonet was provided by Federal Emergency Management Agency grant FEMA-4085-DR-NY, with the continued support of the NYS Division of Homeland Security & Emergency Services; the state of New York; the Research Foundation for the State University of New York (SUNY); the University at Albany, SUNY; the Atmospheric Sciences Research Center (ASRC) at SUNY Albany; and the Department of Atmospheric and Environmental Sciences (DAES) at SUNY Albany. The information related to the NEON network may not have been reviewed or prepared by Battelle. It is provided AS IS without any warranty of any kind, express or implied, and may not reflect Battelle's views or opinions. The research is also funded by The Department of Defense Army Research Office Grant # W911NF-18-1-0371.

References I.

- Chrysoulakis, N., Grimmond, S., Feigenwinter, C. et al. 2018: Urban energy exchanges monitoring from space. *Sci Rep* 8, 11498.
- C.S.B. Grimmond, H.A. Cleugh, T.R. Oke. 1999: An objective urban heat storage model and its comparison with other schemes. *Atmos. Environ. Part B. Urban Atmos.*, 25, pp. 311-326.
- Kato S., Yamaguchi Y. 2007: Estimation of storage heat flux in an urban area using ASTER data. *Remote Sensing of Environment*, 110 (1) , pp. 1-17.
- Offerle, B., Grimmond, C.S.B. and Fortuniak, K. 2005: Heat storage and anthropogenic heat flux in relation to the energy balance of a central European city centre. *Int. J. Climatol.*, 25: 1405-1419.
- Pardyjak E.R. 2019: Environmental Fluid Dynamics - LUMPS Project. <https://my.mech.utah.edu/~pardyjak/efd/murray.html>
- Ramamurthy, P., and Bou-Zeid, E. (2017: Heatwaves and urban heat islands: A comparative analysis of multiple cities, *J. Geophys. Res. Atmos.*, 122, 168– 178.
- Ramamurthy P., Pardyjak E.R. 2011: Toward understanding the behavior of carbon dioxide and surface energy fluxes in the urbanized semi-arid Salt Lake Valley, Utah, USA. *Atmospheric Environment*, 45 (1) , pp. 73-84.

References II.

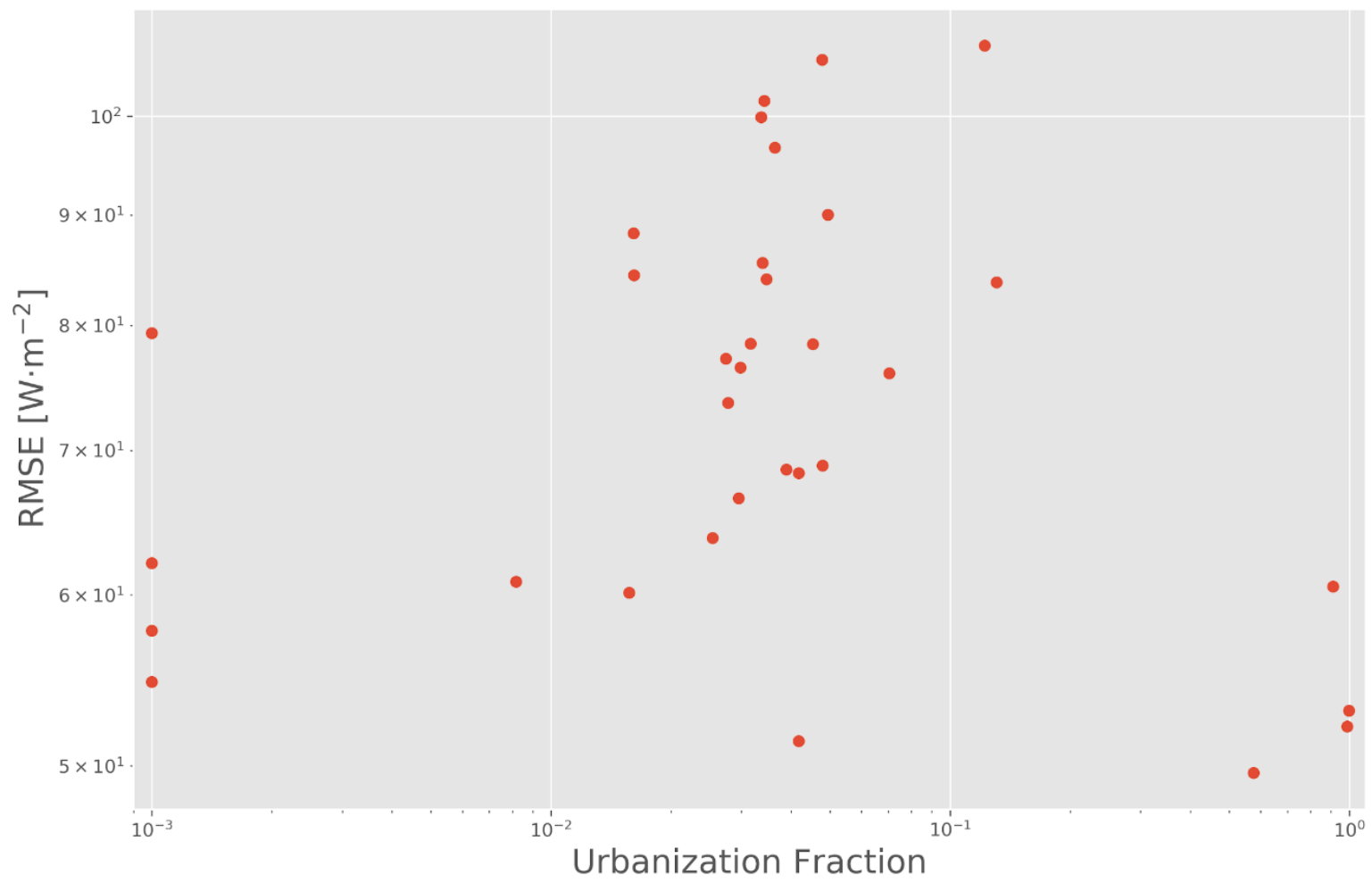
- Roberts, S.M., T.R. Oke, C.S. Grimmond, and J.A. Voogt, 2006: Comparison of Four Methods to Estimate Urban Heat Storage. *J. Appl. Meteor. Climatol.*, 45, 1766–1781.
- Rigo, G., Parlow, E. 2007: Modelling the ground heat flux of an urban area using remote sensing data. *Theor. Appl. Climatol.* 90, 185–199.
- Sailor, D. J. 2002: Urban Heat Islands, Opportunities and Challenges for Mitigation and Adaptation. Sample Electric Load Data for New Orleans, LA (NOPSI, 1995). North American Urban Heat Island Summit. Toronto, Canada. 1–4 May 2002. Data courtesy Entergy Corporation.
- Taha, H., 1999: Modifying a Mesoscale Meteorological Model to Better Incorporate Urban Heat Storage: A Bulk-Parameterization Approach. *J. Appl. Meteor.*, 38, 466–473.
- United States Environmental Protection Agency. <https://www.epa.gov/heat-islands/heat-island-impacts>



Thank you!

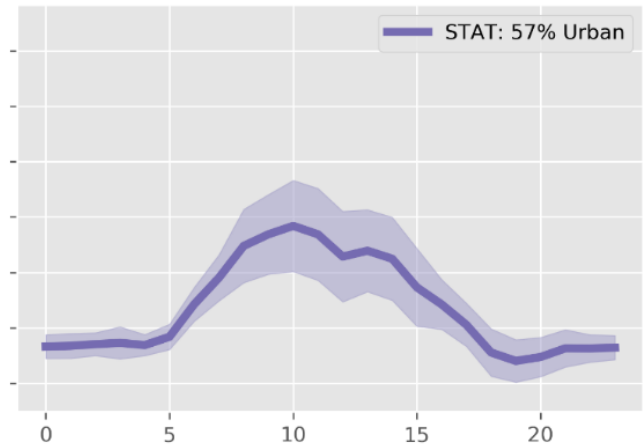
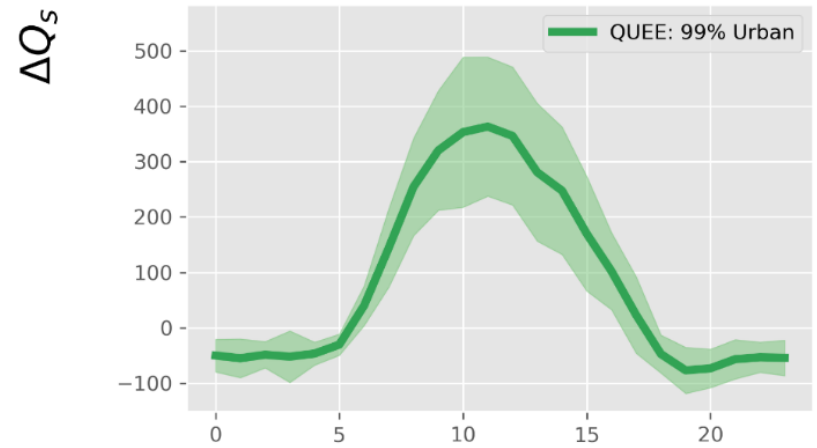
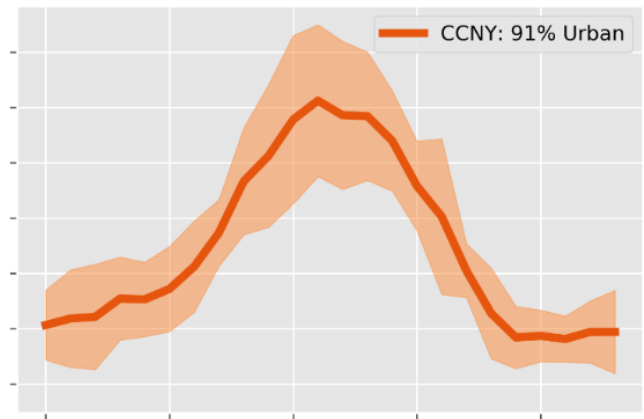
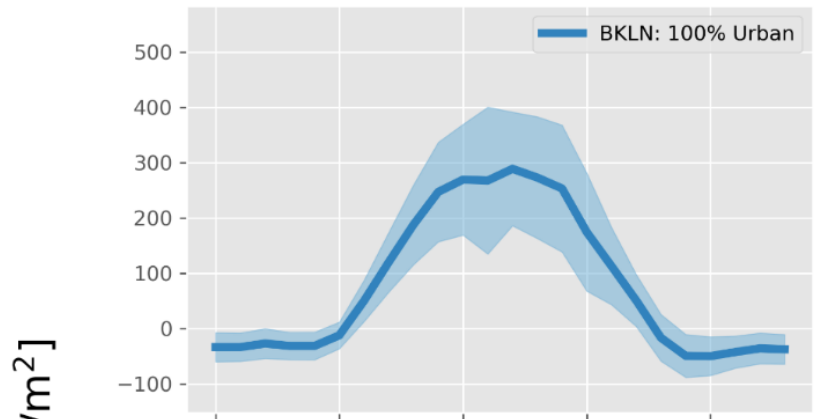
QUESTIONS?

28 Station Mean RMSE: 73.5 [W·m⁻²]





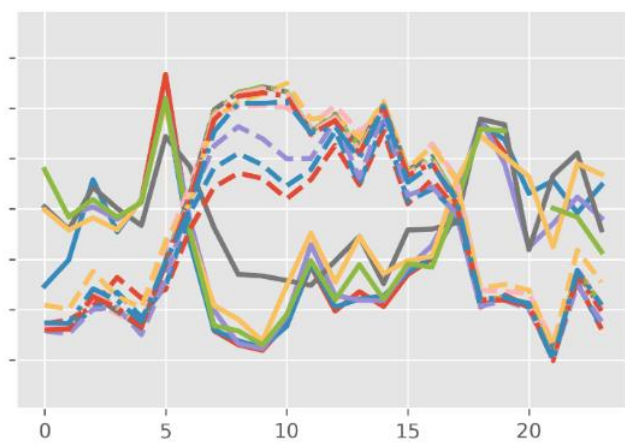
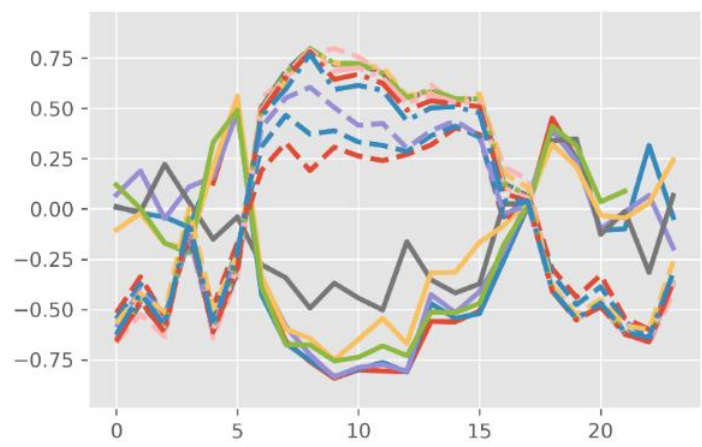
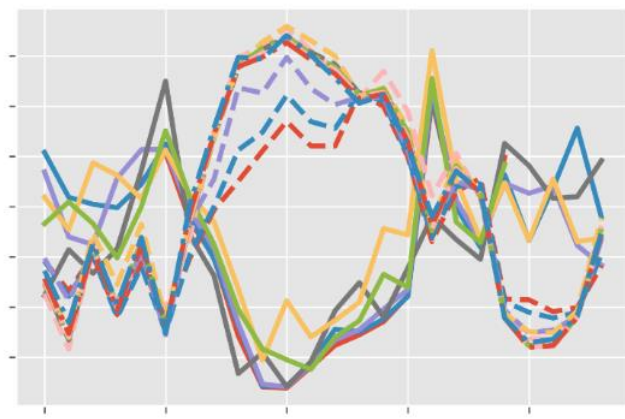
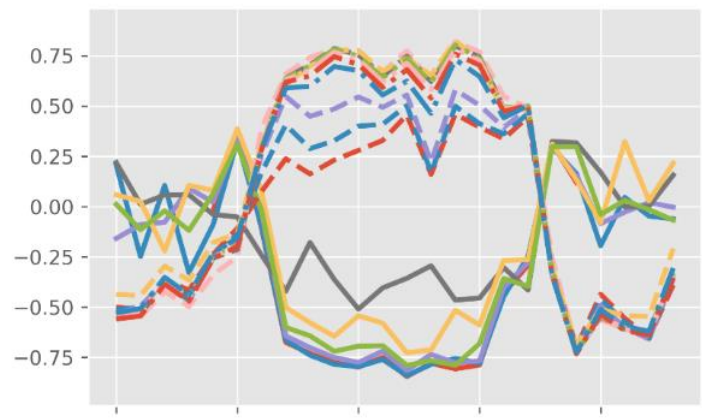
EXTRAS



Hour of Day

Band #	Wavelength [μm]	Resolution [km]	Application
1	0.47	1	detects reflected visible solar radiation.
2	0.64	0.5	detects reflected visible solar radiation
3	0.86	1	Veggie band
4	1.37	2	Detect dust and cloud
5	1.6	1	Fire detection, snow, moisture from clouds
6	2.2	2	Clouds, aerosol optical depth
7	3.9	2	Low-level winds, clouds, fog
8	6.2	2	Winds and Total Precipitable Water
9	6.9	2	Mid-level water vapor, TPW, cloud mask
10	7.3	2	Lower-level water vapor, rain
11	8.5	2	Cloud-top phase and SO ₂
12	9.6	2	ozone
13	10.3	2	vertical temperature/moisture profiles, SST
14	11.2	2	Aerosol and Land Surface Temperature
15	12.3	2	LST & ash and dust
16	13.3	2	CO ₂ , pressure, temperatures

Corr ($\Delta Q_{s_i, L_\lambda}$)



- Band: 1
- Band: 2
- Band: 3
- Band: 4
- Band: 5
- Band: 6
- - - Band: 7
- - - Band: 8
- - - Band: 9
- - - Band: 10
- - - Band: 11
- - - Band: 12
- - - Band: 13
- - - Band: 14
- - - Band: 15
- - - Band: 16

Hour of Day

Table 3. Absolute differences (bias) between in-situ and the modelled ground heat flux densities at six sites (a) with CAR, b) with NDVI and c) with OHM). Values in parentheses represent hypothetical rural differences for the CAR approach

Sites	Mean absolute differences (MAD) between modelled and measured ground heat fluxes in W/m ²						MAD
	U1 Sperr.	U2 Spalen.	U3 Messe	S1 Allschwil	R2 V-Neuf	R3 L Erlen	
a) LANDSAT 08.07.02	4	19	103		(44)	(15)	
a) MODIS day 08.07.02	1	32	96		(36)	(13)	
b) LANDSAT 08.07.02	3	26	1	18	2	69	20
b) MODIS day 08.07.02	1	25	3	9	3	74	19
c) MODIS night/MODIS day 08.07.02	15	4	11	22	20	5	13
c) MODIS night/LANDSAT 08.07.02	1	11	2	4	14	1	5
c) MODIS night/AVHRR 16 day 08.07.02	1	12	5	5	16	1	7
c) MODIS night/AVHRR 14 08.07.02	4	7	0	3	6	1	
c) MODIS night/AVHRR 16 night	6	5	2	7	1	3	4
c) MODIS day/LANDSAT 08.07.02	26	21	78	8	31	2	23
c) MODIS day/AHVRR 14 08.07.02	27	20	71	13	26	2	27
c) MODIS day/AVHRR 16 night 08.07.02	25	18	69	10	21	2	24
c) AVHRR 16 day/AVHRR 14 08.07.02	17	40	24	15	3	11	15
c) AVHRR 16 day/AVHRR 16 night	11	25	24	15	3	11	15
c) LANDSAT/AVHRR 14 08.07.02	5	17	8	10	5	3	8
c) LANDSAT/AVHRR 16 night 08.07.02	7	6	7	14	1	2	6
c) AVHRR 14/AVHRR 16 night 08.07.02	25	54	33	4	9	22	24
c) AVHRR 16/AVHRR 15 25.06.02	30	15	7	10	27	6	16
c) MODIS day/AVHRR 15 25.06.02	39	10	76	9	16	1	25
c) AVHRR16/MODIS day 25.06.02	15	28	19	36	44	9	25
c) AVHRR 16/MODIS day 26.06.02	14	37	7	40	37	12	25
c) MODIS night/AVHRR16 26.06.02	13	24	9	15	18	1	13
c) MODIS night/MODIS day 26.06.02	15	22	9	13	17	1	13
Site mean absolute difference	13	21	29	13	15	11	17
RMSE	11	12	34	10	13	21	17

“Net radiation gave a RMS error of 25 [W· m⁻²]”

A similar satellite method uses MODIS/LANDSAT with MAD: 21.0 [W · m⁻²]



Our MAD: 40.9 [W· m⁻²]

Rigo, G., Parlow, E. Modelling the ground heat flux of an urban area using remote sensing data. *Theor. Appl. Climatol.* 90, 185–199 (2007)

“shortwave upward radiation was derived using linear regression between in-situ measurements...and a channel computed from the visible and near infrared channels of LANDSAT ETM+”